**TITLE**

Translational adaptation to heat stress is mediated by RNA 5-methylcytosine in *Caenorhabditis elegans*

**AUTHORS**

Isabela Cunha Navarro[1,2], Francesca Tuorto[3,4,5], David Jordan[1,2], Carine Legrand[3], Jonathan Price[1,2], Fabian Braukmann[1,2], Alan G. Hendrick[6], Alper Akay[1,2,7], Annika Kotter[8], Mark Helm[8], Frank Lyko[3], Eric A. Miska[1,2,9*]

**AFFILIATION**

1. Gurdon Institute, University of Cambridge, Cambridge, CB2 1QN, UK
2. Department of Genetics, University of Cambridge, Cambridge, CB2 3EH, UK
3. Division of Epigenetics, DKFZ-ZMBH Alliance, German Cancer Research Center, Heidelberg, Germany
4. Division of Biochemistry, Mannheim Institute for Innate Immunoscience (MI3), Medical Faculty Mannheim, Heidelberg University, Mannheim, Germany
5. Center for Molecular Biology of Heidelberg University (ZMBH), DKFZ-ZMBH Alliance, Heidelberg, Germany
6. STORM Therapeutics Limited, Moneta Building, Babraham Research Campus, Cambridge, CB22 3AT, UK
7. School of Biological Sciences, University of East Anglia, Norwich, NR4 7TJ, UK
8. Institute of Pharmacy and Biochemistry, Johannes Gutenberg-University Mainz, 55128 Mainz, Germany
9. Wellcome Sanger Institute, Wellcome Genome Campus, Cambridge, CB10 1SA, UK

*To whom correspondence should be addressed: eam29@cam.ac.uk

## ABSTRACT

Methylation of carbon-5 of cytosines ($m^5C$) is a post-transcriptional nucleotide modification of RNA found in all kingdoms of life. While individual $m^5C$-methyltransferases have been studied, the impact of the global cytosine-5 methylome on development, homeostasis and stress remains unknown. Here, using *Caenorhabditis elegans*, we generated the first organism devoid of $m^5C$ in RNA, demonstrating that this modification is non-essential. Using this genetic tool, we determine the localisation and enzymatic specificity of $m^5C$ sites in the RNome *in vivo.* We find that NSUN-4 acts as a dual rRNA and tRNA methyltransferase in *C. elegans* mitochondria. In agreement with leucine and proline being the most frequently methylated tRNA isoacceptors, loss of $m^5C$ impacts the decoding of some triplets of these two amino acids, leading to reduced translation efficiency. Upon heat stress, $m^5C$ loss leads to ribosome stalling at UUG triplets, the only codon translated by an $m^5C34$-modified tRNA. This leads to reduced translation efficiency of UUG-rich transcripts and impaired fertility, suggesting a role of $m^5C$ tRNA wobble methylation in the adaptation to higher temperatures.

**Keywords:** *Caenorhabditis elegans* / 5-methylcytosine / NSUN / RNA modifications / translation efficiency

## INTRODUCTION

The methylation of carbon-5 of cytosines ($m^5C$) in RNA is a conserved modification in biological systems. $m^5C$ has been detected in tRNAs, rRNAs, mRNAs and non-coding RNAs, and is catalysed by $m^5C$ RNA-methyltransferases that utilise SAM as a methyl donor (Liu & Santi, 2000; Boccaletto *et al*, 2017). In humans, RNA $m^5C$ formation is catalysed by the tRNA aspartic acid MTase 1 (TRDMT1/DNMT2), and by seven proteins of the NOP2/Sun domain family (NSUN1-7) (García-Vílchez, *et al*, 2019). Pathogenic mutations in humans have been mapped to several genes involved in the $m^5C$ pathway (Abbasi-Moheb *et al*, 2012; Haag *et al*, 2016; Khan *et al*, 2012; Khosronezhad *et al*, 2015; Komara *et al*, 2015; Martinez *et al*, 2012; Nakano *et al*, 2016; Ren *et al*, 2015; Van Haute *et al*, 2016). Despite its conservation and clear relevance, the functions and molecular interactions of the RNA $m^5C$ methylome remain largely unknown. Here, we use *Caenorhabditis elegans* as a model to study the genetic requirements and molecular functions of $m^5C$ modification and its methyltransferases *in vivo*.

67 $m^5C$ has been implicated in a variety of molecular roles. Amongst the most highly
68 modified methyltransferase targets are tRNAs and rRNAs, the core components of the
69 translation machinery. tRNAs are methylated by NSUN2, NSUN3, NSUN6 and DNMT2,
70 while rRNAs are methylated by NSUN1, NSUN4 and NSUN5 (García-Vílchez *et al*, 2019).
71
72 In some tRNAs, $m^5C$ protects from degradation. Loss of NSUN2-mediated tRNA
73 methylation has been shown to promote cleavage by angiogenin and accumulation of tRNA
74 fragments that interfere with the translation machinery (Flores *et al*, 2016; Blanco *et al*, 2014,
75 2016; Tuorto *et al*, 2012). Similarly, DNMT2-mediated methylation was found important for
76 protection of tRNAs from stress-induced cleavage in *Drosophila* and mice (Schaefer *et al*,
77 2010; Tuorto *et al*, 2015, 2012). NSUN6-mediated methylation of tRNAs Cys and Thr
78 promotes a slight enhancement of tRNA thermal stability (Haag *et al*, 2015; Li *et al*, 2018)
79
80 In other tRNAs, $m^5C$ modulates translational fidelity. DNMT2 has been shown to
81 facilitate charging of tRNA Asp and discrimination between Asp and Glu near-cognate codons,
82 thus controlling the synthesis of Asp-rich sequences and promoting translational fidelity
83 (Tuorto *et al*, 2015; Shanmugam *et al*, 2015). NSUN3 methylates exclusively mitochondrial
84 tRNA Met-CAU at the wobble position, which is further modified into $f^5C$ by the dioxygenase
85 ALKBH1, facilitating the recognition of AUA and AUG codons as methionine in the
86 mitochondria (Van Haute *et al*, 2016; Nakano *et al*, 2016; Haag *et al*, 2016; Takemoto *et al*,
87 2009). Lack of $f^5C$ affects mitochondrial translation rates in human fibroblasts (Van Haute *et*
88 *al*, 2016).
89
90 The rRNA methyltransferase NSUN1 (yeast *nop2*) methylates C2870 in yeast 25S
91 rRNA. While NSUN1 is an essential gene in all organisms studied thus far, it remains unclear
92 whether this is dependent on its catalytic activity (Sharma *et al*, 2013). Similarly, NSUN4 acts
93 in complex with MTERF4 for assembly of small and large mitochondrial ribosome subunits,
94 however $m^5C$ catalysis does not seem to be essential (Metodiev *et al*, 2014). NSUN5 has been
95 shown to methylate position C2278 in yeast 25S rRNA (Schosserer *et al*, 2015; Sharma *et al*,
96 2013). Loss of NSUN5-mediated methylation induces conformational changes in the ribosome
97 and modulation of translational fidelity, favouring the recruitment of stress-responsive mRNAs
98 into polysomes and promoting lifespan enhancement in yeast, flies and nematodes. In
99 mice, Nsun5 knockout causes reduced body weight and reduced protein synthesis in several
100 tissues (Schosserer *et al*, 2015; Heissenberger *et al*, 2019).

101

102 It remains less clear whether mRNAs are specific targets of $m^5C$-methyltransferases
103 and if $m^5C$ is functional in mRNA. Several methods have been used to investigate the presence
104 and function of $m^5C$ in coding transcripts and two $m^5C$-binding proteins have been identified
105 so far (Chen *et al*, 2019; Yang *et al*, 2017). However, there is a lack consensus on the
106 abundance, distribution and relevance of this mark in mRNAs, as the number and identity of
107 putative mRNA $m^5C$ sites varies widely between studies (David *et al*, 2017; Huang *et al*, 2019;
108 Legrand *et al*, 2017; Li *et al*, 2017; Squires *et al*, 2012; Tang *et al*, 2015; Yang *et al*, 2017;
109 Zhang *et al*, 2012).

110

111 Although previous studies have explored the roles of individual $m^5C$
112 methyltransferases, none have established a systematic dissection of these enzymes as a class,
113 of their specificity, or of their potential molecular and genetic interactions, in any organism.
114 Many questions remain on how the $m^5C$ methylome sustains development and normal
115 physiology. In this work, we generated the first mutant animals devoid of any detectable levels
116 of cytosine C5 methylation in RNA, demonstrating that $m^5C$ is a non-essential modification
117 under standard conditions. We then used this mutant strain as genetic tool to map $m^5C$ sites
118 onto RNA *in vivo* and determined their impact on translation, development, physiology and
119 stress.

120

121 **RESULTS**

122

123 **$m^5C$ and its derivatives are non-essential RNA modifications in *C. elegans***

124 To identify putative $m^5C$ RNA methyltransferases in *C. elegans,* we performed a BLAST
125 analysis and found that the open reading frames *W07E6.1*, *Y48G8AL.5*, *Y39G10AR.21* and
126 *Y53F4B.4* are likely homologues of the human genes NSUN1, NSUN2, NSUN4 and NSUN5,
127 respectively (**Fig 1A**). Knockdown of these genes through RNAi by feeding revealed that *nsun-*
128 *1* is an essential gene, as 100% of the animals that had this gene silenced from the first larval
129 stage onwards developed into sterile adults (**Fig 1B, C**). We could not identify homologous
130 genes of NSUN3, NSUN6, NSUN7 or DNMT2.

131

132 $m^5C$ RNA methyltransferases utilise two conserved cysteine residues for the methyl
133 group transfer, one of which (TC-Cys) is required for the covalent adduct formation, and the
134 other (PC-Cys) for the release of the substrate following $m^5C$ catalysis (King & Redman,

135 2002). Using CRISPR-Cas9, we introduced mutations converting the TC-Cys into alanine in
136 *nsun-1* (*mj473*), *nsun-2* (*mj458*) and *nsun-4* (*mj457*) (**Fig 1D, Appendix Fig S1A, B**). These
137 mutants, as well as a previously reported knockout mutant of *nsun-5* (*tm3898*), are viable and
138 produce viable progeny, suggesting that the individual activity of $m^5C$ methyltransferases is
139 not essential for the viability of *C. elegans*. In addition, these results suggest that the essential
140 role played by NSUN-1 in fertility (**Fig 1B, C**) is independent of the catalytic functions of this
141 protein.
142
143 To investigate epistatic interactions among the *nsun* genes in *C. elegans*, we performed
144 genetic crosses between the individual mutants, and produced a quadruple mutant in which all
145 *nsun* genes are predicted to be inactive. This strain was viable and fertile, and was termed
146 noNSUN. To confirm whether the introduced mutations resulted in catalytic inactivation, and
147 to rule out the existence of additional unknown $m^5C$ RNA methyltransferases, we performed
148 mass spectrometry analyses in total RNA from the mutant strains, and confirmed that $m^5C$ is
149 no longer detectable in this genetic background (**Fig 1E**; lower limit of detection ~0.3 ng/ml,
150 average amount detected in wild type samples 477 ng/ml). We additionally quantified the $m^5C$
151 metabolic derivative 2′-O-methyl-5-hydroxymethylcytosine ($hm^5Cm$) (Huber, *et al*, 2017) and
152 found that this modification is not present either in *nsun-2* or noNSUN mutants (**Fig 1F**). We
153 therefore conclude that $m^5C$ and its derivatives are not essential for *C. elegans* viability under
154 laboratory conditions. Furthermore, we showed that NSUN-2 is the main source of $m^5C$ (88%
155 of total), and that $hm^5Cm$ sites exclusively derive from NSUN-2 targets in *C. elegans*.
156
157 It has been proposed that some RNA modifications may act in a combinatorial manner,
158 providing compensatory effects to each other (Hopper & Phizicky, 2003). This prompted us to
159 investigate whether complete loss of $m^5C$ would significantly interfere with the levels of other
160 RNA modifications. We performed a mass spectrometry analysis to quantify 15 different
161 modifications in total RNA and found no significant differences between wild type and
162 noNSUN samples (**Fig 1G**). Taken together, our data establish the noNSUN strain as a highly
163 specific genetic tool for the study of $m^5C$ distribution and function *in vivo*.
164
165 **The $m^5C$ methylome of *C. elegans***
166 Schosserer *et al* demonstrated that position C2381 of 26S rRNA is methylated at carbon-5 by
167 NSUN-5 in *C. elegans*, being involved in lifespan modulation (Schosserer *et al*, 2015).
168 Nevertheless, the $m^5C$ methylome of this organism remained to be determined. We therefore

169 used the noNSUN strain as a negative control for whole-transcriptome bisulfite sequencing
170 (WTBS) analysis (Legrand *et al*, 2017), aiming to determine the localisation of $m^5C$ sites in *C.*
171 *elegans* RNA at single nucleotide resolution.
172
173 We identified C5 methylation at positions C2982 and C2381 of 26S cytoplasmic rRNA
174 and positions C628 and C632 of 18S mitochondrial rRNA (**Fig 2A**). Using alignment to rRNA
175 of different organisms we found that position C2982 is a conserved NSUN1 target (Sharma *et*
176 *al*, 2013), which has also been recently reported in *C. elegans* (Heissenberger *et al*, 2020). In
177 addition, C2381 has previously been reported as a conserved NSUN5 target (Schosserer *et al*,
178 2015; Sharma *et al*, 2013). We further confirmed the specificity of these sites using a targeted
179 bisulfite sequencing (BS-seq) approach in individual mutants (**Fig EV1A, B**). Interestingly,
180 other groups had previously identified adjacent modified sites in mt-rRNA in mice, however
181 the methylation of only one of the positions was shown to be dependent on NSUN4 activity,
182 while the other was interpreted as a 4-methylcytosine site (Metodiev *et al*, 2014). In the case
183 of *C. elegans*, both positions are NSUN-dependent (**Fig 2A**).
184
185 We found 40 positions to be methylated in stoichiometry higher than 50% in tRNAs,
186 the majority of which being detected in leucine and proline isoacceptors (**Fig 2B-C**). As
187 anticipated for NSUN2 targeting, modified positions are found in the variable loop region
188 (positions 48, 49, 50), with cytoplasmic tRNA Leu-CAA carrying an additional modification
189 at the wobble position (C34) (Blanco *et al*, 2014; Burgess, *et al*, 2015) (**Fig 2C**). Using targeted
190 BS-seq, we demonstrated that NSUN-2 is indeed responsible for both C34 and C48 methylation
191 in tRNA-Leu (**Fig EV1C**). In agreement with the lack of homologous genes of DNMT2 and
192 NSUN6 in *C. elegans*, no methylation was found on conserved RNA targets of these enzymes
193 (Goll *et al*, 2006; Schaefer *et al*, 2010; Long *et al*, 2016) (**Fig 2C**).
194
195 Contrasting with what was observed for tRNAs and rRNAs, non-conversion of mRNA
196 sites in *C. elegans* is rare and occurs at much lower stoichiometry. Lowering the non-
197 conversion threshold from 50% to 25-40%, we detected 188 positions that remained
198 unconverted after bisulfite treatment exclusively in wild type samples, *i.e.* putative $m^5C$ sites
199 (**Fig 2D**, x axis). Using the same thresholds to probe for likely artefacts revealed 88 positions
200 that remained unconverted exclusively in noNSUN samples, *i.e.* non-conversion was only 46%
201 less frequent (**Fig 2D,** y axis). It is also noteworthy that positions remaining reproducibly
202 highly unconverted equally in wild type and noNSUN samples are more frequent in mRNAs,

203 when compared to tRNAs and rRNAs (**Fig 2A-B, D**). In summary, we found no evidence of a
204 widespread distribution of $m^5C$ in coding transcripts. To investigate whether the presence of
205 common characteristics could support a subset of the aforementioned 188 positions as *bona*
206 *fide* methylated sites, we performed gene ontology, motif search, genomic localisation, and
207 secondary structure analyses on these transcripts and sites, however no significant shared
208 features were found. While our data does not completely rule out the existence of $m^5C$
209 methylation in mRNAs, it demonstrates that this mark cannot be detected in high stoichiometry
210 in *C. elegans*, as observed in tRNAs and rRNAs.
211
212 Finally, we attempted to identify $m^5C$ sites in small RNAs in our dataset. Given that
213 the fractionation used in this protocol aimed to enrich for tRNAs (60-80 nt), we could not detect
214 microRNA reads in abundance for confident analysis. Nevertheless, we found high NSUN-
215 dependent non-conversion rates (>80%) in five non-coding RNAs (approximately 60 nt long)
216 previously identified in *C. elegans* (Lu *et al*, 2011; Xiao *et al*, 2012) (Figure 2E). Secondary
217 structure predictions suggest that the methylated sites are often found on the base of a stem-
218 loop, reminiscent of tRNA variable loops (**Fig EV2**). Further experiments will be required to
219 determine the functionality of these $m^5C$ sites.
220
221 **NSUN-4 is a multisite-specific tRNA/rRNA-methyltransferase in the mitochondria of**
222 ***C. elegans***
223 Interestingly, we found the mitochondrial tRNA Met-CAU to be methylated at a very high rate
224 (94.7%) (**Fig 3A**). Supporting our finding, previous articles also indicated the detection of this
225 modified site in *Ascaris suum* and *C. elegans* (Nakano *et al*, 2016; Watanabe *et al*, 1994). This
226 was unexpected, as previous reports have shown that this position is methylated by NSUN3
227 (Haag *et al*, 2016; Nakano *et al*, 2016; Van Haute *et al*, 2016). As *C. elegans* does not have an
228 NSUN3 homologue, this implies that mitochondrial tRNAs can be modified by alternative
229 enzymes. A BLAST analysis of the human NSUN3 methyltransferase domain against the *C.*
230 *elegans* proteome showed higher similarity to NSUN-4 (30% identity), followed by NSUN-2
231 (26% identity). Moreover, we observed that, among human NSUN genes, NSUN3 and NSUN4
232 share the highest percentage of similarity (**Fig 3B**). Using a targeted BS-seq approach, we
233 probed the methylation status of position C34 in mitochondrial tRNA Met-CAU from wild
234 type, *nsun-2* and *nsun-4* strains. Our results indicate that NSUN-4 is responsible for the
235 catalysis of $m^5C$ in this position in *C. elegans* (**Fig 3C**).
236

237 NSUN-4 is the only mitochondrial rRNA $m^5C$ methyltransferase identified to date. To
238 confirm that the previously reported role of NSUN4 is also conserved in *C. elegans*, we
239 performed targeted BS-seq in 18S mitochondrial rRNA, and found that methylation of
240 positions C628 and C632, as well as C631, is mediated by NSUN-4 (**Fig 3D**). Notably,
241 methylation of position C631 was also detected by WTBS, however in reduced stoichiometry
242 (23.5% in wild type vs. 0.04% in noNSUN). Taken together, our results show that NSUN-4 is
243 a multisite-specific tRNA/rRNA mitochondrial methyltransferase in nematodes.
244
245 To investigate when the divergence of NSUN3 arose in evolution, a phylogenetic
246 analysis of NSUN3 was performed using Treefam and, given the high sequence similarity,
247 NSUN3 and NSUN4 sequences were automatically included in the generated cladogram.
248 While *Drosophila* and *C. elegans* only have NSUN4, vertebrate model organisms as basal as
249 zebrafish have both NSUN3 and NSUN4 (Fig 3E). A more expanded version of the tree
250 indicates the presence of NSUN4, but not NSUN3, in sea lampreys
251 (http://www.treefam.org/family/TF321304#tabview=tab1), suggesting that NSUN3 diverged
252 from NSUN4 in vertebrates.
253
254 **Loss of $m^5C$ leads to temperature-sensitive reproductive phenotypes**
255 The individual or collective introduction of mutations in *nsun* genes failed to induce noticeable
256 abnormal phenotypes. We therefore performed a more extensive characterisation of the mutant
257 strains using a live imaging-based phenotypic analysis (Akay *et al*, 2019). As a proxy for
258 reduced fitness, we chose to analyse the number of viable progeny and occurrence of
259 developmental delay (growth rate, as measured by body length). In comparison to wild type
260 animals, we observed a delay in all mutant strains, which persists throughout development and
261 into adulthood. This difference is greater in noNSUN animals, especially as this strain
262 transitions from L4 stage to young adulthood (**Fig 4A**). When comparing mutants' sizes at
263 young adult stage at 20°C, noNSUN animals are, on average, five times smaller than wild type
264 (**Fig 4B**). While this difference reflects a developmental delay, noNSUN animals remain 20%
265 smaller even when they reach adulthood themselves (**Fig 4B**). In addition, the noNSUN strain
266 shows a 25% reduction in brood size, which is comparable to what is observed in *nsun-1* and
267 *nsun-5* individual mutants (**Fig 4C**).
268
269 *C. elegans* stocks can be well maintained between 16°C and 25°C, being most typically
270 kept at 20°C. To gain insights into how the loss of $m^5C$ impacts development under different

271 environmental conditions, wild type and noNSUN animals were cultured at 25°C for three
272 generations and subjected to automated measurements. As shown in **Fig 4D**, the reproductive
273 phenotype previously observed in the noNSUN strain (**Fig 4C**) is significantly aggravated at
274 this temperature. This suggests that the phenotypes arising from loss of $m^5C$ are temperature-
275 sensitive, pointing towards an involvement of this modification in the adaptation to
276 environmental changes.
277
278 **Loss of $m^5C$ impacts translation efficiency of leucine and proline codons**
279 To explore the impact of temperature stress in the absence of $m^5C$ while avoiding the
280 confounding effect introduced by differences in brood size, we performed further experiments
281 using an acute heat shock treatment. To investigate whether the observed phenotypes are linked
282 to abnormalities in protein translation rates, we quantified the polysomal fraction in wild type
283 and noNSUN adult animals subject to heat shock at 27°C for 4 hours and found no significant
284 differences (**Fig 5A, Appendix Fig S2**).
285
286 To gain insights into transcriptional and translational differences resulting from the loss
287 of $m^5C$, we performed transcriptomic and ribosome profiling analyses. The latter allows the
288 quantification of active translation by deep-sequencing of the mRNA fragments that are
289 protected from nuclease digestion by the presence of ribosomes (ribosome protected fragments
290 - RPFs). RPFs showed the expected 3 nt periodicity along the coding domain sequences of
291 mRNA, with the majority of reads in frame **(Appendix Fig S3A, B).** Furthermore, RNASeq
292 and riboSeq counts of genes showed high correlation, and variation in the gene counts could
293 be attributed to the difference in samples analysed (**Appendix Fig S3C, D, E**). Loss of $m^5C$
294 did not greatly impact the nature of the heat stress response, as most differentially transcribed
295 and translated genes upon heat stimulus showed agreement, or very subtle differences between
296 wild type and noNSUN strains (**Appendix Fig S4**). We found that differentially transcribed
297 genes upon loss of $m^5C$ are mainly involved in cuticle development (**Fig EV3A**), while
298 differentially translated genes are enriched in components of the cuticle and ribosomes, as well
299 as RNA-binding proteins (**Fig EV3B**).
300
301 We then evaluated genome-wide codon occupancy during translation elongation in
302 both temperatures and found that loss of $m^5C$ leads to increased ribosome occupancy at leucine
303 and proline codons. Upon heat shock, Leu-UUG codons showed the highest ribosome density
304 observed in the noNSUN strain, suggesting that translation of this codon is slowed during heat

305 stress in the absence of $m^5C$ (**Fig 5B, Fig EV4A**). We investigated this phenomenon more
306 closely in different transcripts and found that ribosome stalling at UUG codons seems to be
307 context-dependent, as it only occurs in a small subset of UUG codons (**Fig 5C**, **Fig EV4B**).
308 Interestingly, as shown in our WTBS analysis, leucine and proline are the most frequently
309 methylated tRNA isoacceptors in *C. elegans* (**Fig 2B**). In addition, tRNA Leu-CAA,
310 responsible for decoding of UUG codons, is the only cytoplasmic tRNA bearing an $m^5C$-
311 modified wobble position (**Fig 2C**).
312
313 As a downstream consequence of ribosome stalling, we found translation efficiency of
314 UUG-, leucine- and proline-rich genes to be significantly reduced in the noNSUN strain. While
315 this effect can be observed in both temperatures in leucine-rich transcripts and at 20°C in
316 proline-rich ones, it occurs in a heat shock-dependent manner in UUG-rich transcripts,
317 suggesting an involvement of $m^5C$ wobble methylation in the adaptation to heat stress (**Fig**
318 **5D**). Finally, we found that translation efficiency is further reduced as transcripts get more
319 enriched in the affected codons (**Fig EV5**).
320
321
322 **DISCUSSION**
323 Chemical modifications of RNA occur in organisms from all kingdoms of life and are often
324 highly conserved throughout evolution, as is the case of the methylation of carbon-5 in
325 cytosines (Boccaletto *et al*, 2017; Huber *et al*, 2015). Despite that, there is a growing body of
326 evidence showing that several RNA modifications are individually not required for
327 development under controlled conditions (O'Connor, *et al* 2018, reviewed in Sharma &
328 Lafontaine, 2015 and Hopper & Phizicky, 2003). Our results reignite a recurrent question in
329 the epitranscriptomics field: why are so many of these chemical marks extensively conserved
330 throughout evolution and, yet, organisms often present subtle phenotypes in their absence?
331 Ribonucleoside modifications occur in an overwhelming diversity and, in some cases, might
332 *(i)* exert subtle molecular effects, *(ii)* act in a combinatorial or redundant manner with other
333 modifications or *(iii)* be the result of relaxed enzymatic specificity (Phizicky & Alfonzo, 2010;
334 Jackman & Alfonzo, 2013).
335
336 While the absence of $m^5C$ in RNA did not give rise to overt phenotypes under standard
337 laboratory conditions, a more detailed analysis of the mutants revealed developmental and
338 fertility defects. Previous studies have shown that levels of several RNA modifications,

339 including $m^5C$, are responsive and can react dynamically to a wide range of environmental
340 challenges, such as toxicants, starvation and heat shock, thus potentially supporting organismal
341 adaptation (Chan *et al*, 2010; van Delft *et al*, 2017). In agreement with this idea, we observed
342 a temperature-dependent aggravation of reproductive phenotypes in $m^5C$-deficient *C. elegans*.
343 In nature, where the environmental conditions vary greatly, such genotypes would likely be
344 selected against in a wild population.
345
346 Our results suggest an RNA methylation-independent essential role for NSUN-1 in
347 germline development. Consistently, Nop2p/Nol1/NSUN1 has been shown to be an essential
348 gene in yeast, mice and *Arabidopsis* (Burgess *et al*, 2015; De Beus *et al*, 1994; Kosi *et al*, 2015;
349 Sharma *et al*, 2013). In *Saccharomyces cerevisiae*, both depletion and catalytic mutation of
350 Nop2p lead to lower levels of 60S ribosomal subunits, supporting the idea that reduced
351 methylation affects rRNA processing and translation (Hong *et al*, 1997; Hong*et al*, 2001;
352 Sharma *et al*, 2013). In contrast, Bourgeois *et al* reported that loss of Nop2p-mediated $m^5C$ had
353 no effect on ribosome synthesis and phenotype (Bourgeois *et al*, 2015). A similar phenomenon
354 has been observed for NSUN4 in mice, as well as for Dim1 and Trmt12 in yeast, and their
355 human homologues DIMT1L and WBSCR22, where the presence of the enzyme, rather than
356 its catalytic activity, is required for viability (Lafontaine *et al*, 1995; Metodiev *et al*, 2014;
357 Zorbas *et al*, 2015). It has been proposed that the essential binding of certain rRNA
358 methyltransferases represents a quality control step in ribosome biogenesis, committing rRNA
359 to methylation during the maturation process (Lafontaine *et al*, 1998).
360
361 Taking advantage of the noNSUN strain as a tool to increase the confidence of WTBS
362 analysis, we produced the first comprehensive list of $m^5C$ sites throughout *C. elegans*
363 transcriptome. Using a targeted approach, we showed that NSUN-4 has both rRNA and tRNA
364 targeting capabilities in the mitochondria. It has been suggested that binding of MTERF4 and
365 NSUN4 in a complex is responsible for targeting the methyltransferase to rRNA in the
366 mitochondria (Metodiev *et al*, 2014; Spåhr *et al*, 2012; Yakubovskaya *et al*, 2012).
367 Nevertheless, genetic evidence suggests that NSUN4 methylates rRNA independently of
368 MTERF4 in mice (Metodiev *et al*, 2014). *C. elegans* has an MTERF4 homologue (K11D2.5),
369 and most residues involved in the interaction with NSUN4 appear conserved, suggesting that
370 a similar interaction with this co-factor could occur (Spåhr *et al*, 2012).
371

372 In humans, NSUN3-mediated methylation at position 34 of mitochondrial tRNA Met-
373 CAU is further modified by the dioxygenase ALKBH1 to form $f^5C$ (Haag *et al*, 2016; Nakano
374 *et al*, 2016). Previous studies explored differential methods for the detection of $f^5C$, indicating
375 that 35-100% of tRNA Met-CAU molecules are $f^5C$-modified, while the whole population is
376 at least $m^5C$-modified (Haag *et al*, 2016; Kawarada *et al*, 2017; Van Haute *et al*, 2016). As
377 $f^5C$ reacts as an unmodified cytosine upon sodium bisulfite treatment, it was surprising to detect
378 high levels of non-conversion (95%) in our study. Nakano *et al* (2016) have used DNA probes
379 in reciprocal circulating chromatography followed by mass spectrometry to demonstrate high
380 stoichiometry of $f^5C$ in this site in *C. elegans* RNA. In addition, an ALKBH1 homologue
381 (Y51H7C.5) has recently been discovered and implicated in mitochondrial protein biogenesis
382 in the nematode (Wagner *et al*, 2019). These results support the existence of a $f^5C$ pathway in
383 *C. elegans*. However, as we used a sequencing-based method that does not discriminate
384 between precursors or mature tRNAs, it is possible that our method detects mainly primary
385 transcripts or precursor molecules, which have not been oxidised by ALKBH1.
386
387 Using the noNSUN strain as a negative control, we investigated the presence of $m^5C$ in
388 coding transcripts. Several reports have shown that $m^5C$ is a common mRNA modification
389 (Amort *et al*, 2017; David *et al*, 2017; Squires *et al*, 2012; Yang *et al*, 2017). However, results
390 derived from BS-seq can be influenced by several factors, such as incomplete deamination,
391 protection due to secondary structures, presence of other modifications, protein binding and
392 sequencing errors, among others (summarized in Legrand *et al*, 2017). Given these technical
393 drawbacks, the noNSUN strain represented an unprecedentedly stringent negative control,
394 which allowed for exclusive detection of highly specific methylation. Despite the detection of
395 positions with 20-30% NSUN-dependent non-conversion, we detected a similar number of
396 positions with NSUN-independent non-conversion at these rates, which we interpret as false
397 positives. This poses a statistical challenge on the interpretation of such non-converted
398 positions as methylated. Our main conclusion, therefore, is that the data does not provide
399 evidence for widespread or high stoichiometry $m^5C$ methylation of coding transcripts in *C.*
400 *elegans*. This is in agreement with earlier work using chromatography (Adams & Cory, 1975;
401 Desrosiers *et al*, 1974; Salditt-Georgieff *et al*, 1976) and other reports that have detected very
402 few or no $m^5C$ sites in eukaryotes by BS-seq (Edelheit *et al*, 2013; Khoddami & Cairns, 2013;
403 Khoddami *et al*, 2019; Legrand *et al*, 2017).
404

405 Using ribosome profiling, we investigated the genome-wide effect of loss of $m^5C$ in
406 translational speed and efficiency and found leucine and proline translation to be affected. The
407 strongest effect by far was observed in a heat shock-dependent manner in UUG codons, which
408 rely on the only tRNA modified at the wobble position - tRNA Leu-CAA. Chan *et al* (2012)
409 found that $m^5C$ level specifically at position 34 of tRNA Leu-CAA is upregulated upon
410 oxidative stress in yeast. The presence of this modification was shown to enhance translation
411 efficiency of a UUG-rich luciferase reporter construct, as *trm4*Δ (NSUN2 homologue mutant)
412 cells showed significantly lower levels of reporter activity, especially under oxidative stress.
413 The biological relevance of these findings was linked to an abnormally high frequency of UUG
414 codons in transcripts of specific ribosomal protein paralogues (Chan *et al*, 2012).
415
416 In summary, $m^5C$ supports *C. elegans* fitness at higher temperatures and enhances the
417 translational efficiency of leucine and proline codons in physiology and stress. Our work
418 highlights a specific role of cytosine C5 methylation in facilitating translation of leucine UUG
419 codons upon heat shock, suggesting that $m^5C$ tRNA wobble methylation is involved in the
420 adaptation to heat stress.
421
422
423 **MATERIALS AND METHODS**
424
425 **Genetics**
426 *C. elegans* strains were grown and maintained as described in Brenner (Brenner, 1974). The
427 strains were kept at 20°C, unless otherwise indicated. HB101 strain *Escherichia coli* was used
428 as food source (*Caenorhabditis* Genetics Center, University of Minnesota, Twin Cities, MN,
429 USA). Bristol N2 was used as the wild type strain.
430
431 **Gene silencing by RNAi**
432 Empty vector, *nsun-1* (*W07E6.1*), *nsun-2* (*Y48G8AL.5*), *nsun-4* (*Y39G10AR.21*), and *nsun-5*
433 (*Y53F4B.4*) bacterial feeding clones were kindly provided by Prof. Julie Ahringer's lab
434 (Kamath & Ahringer, 2003). Single colonies were inoculated in LB-Ampicillin 100 µg/ml and
435 cultured for 8 h at 37 °C. Bacterial cultures were seeded onto 50 mm NGM agar plates
436 containing 1 mM IPTG and 25 µg/ml Carbenicillin at a volume of 200 µl of bacterial culture
437 per plate, and left to dry for 48 hours. 50 synchronized L1 larvae were placed onto RNAi plates

438 and left to grow until adult stage. Adults were scored for fertility (presence of embryos in the
439 germline).
440
441 **CRISPR-Cas9 gene editing**
442 CRISPR-Cas9 gene editing was performed as in Paix et al (Paix *et al*, 2015). Briefly, injection
443 mixes were prepared in 5 mM Tris pH 7.5 as follows: 20 µg of tracrRNA (Dharmacon), 3.2 µg
444 of *dpy-10* crRNA (Dharmacon), 200 ng of *dpy-10* homologous recombination template (Sigma
445 Aldrich), 8 µg of target gene gRNA (Dharmacon), 1.65 µg of homologous recombination
446 template (Sigma), up to a volume of 11.5 µl. The mix was added to 10 µg of Cas9 (Dharmacon)
447 to a final volume of 15 µl, and incubated at 37°C for 15 min. For the creation of *nsun* catalytic
448 mutants, a homologous recombination template bearing a point mutation to convert the
449 catalytic cysteine into alanine while creating a restriction site for HaeIII was co-injected.
450 Following incubation, the mix was immediately micro-injected into the germline of N2 young
451 adults. After injection, animals were left to recover in M9 medium, then transferred to
452 individual plates and left to recover overnight at 20°C. Successful injections led to the hatch of
453 dumpy and roller animals. From positive plates, 96 animals were individualized for self-
454 fertilization and genotyped for the relevant alleles. Same process was performed with F2s, until
455 a homozygous population was isolated. Each strain was backcrossed at least three times with
456 the wild type strain.
457
458 **RNA extraction (Mass spectrometry and WTBS)**
459 The strains of interest (N2 and noNSUN) were grown in 90 mm plates until gravid adult stage,
460 washed three times with M9 and pelleted by centrifugation at 2000 rpm for 2 minutes. Gravid
461 adults were resuspended in 4 ml of bleaching solution (final concentration 177 mM NaOH, 177
462 mM NaOCl solution - free chlorine 4–5%) and vortexed vigorously for 7 minutes. Recovered
463 embryos were washed four times to remove any traces of bleach and left to hatch in ml of M9
464 for 24 h at 20°C in a rotating wheel. Synchronised L1 starved larvae were used for RNA
465 extraction. Independent triplicates were obtained from three different generations.
466 Nematodes were washed thoroughly in M9 to remove bacterial residue, and pelleted in RNAse-
467 free tubes at 2000 rpm for 2 min. 500-1000 µl of TRIsure (Bioline) and 100 µl of zirconia beads
468 were added and the samples were subjected to three cycles of 6,500 rpm with 20 sec breaks on
469 Precellys to crack open the animals. 100 µl of chloroform were added to the tubes, which were
470 then shaken vigorously for 15 sec and incubated at room temperature for 3 min. Samples were
471 centrifuged at 12,000 x *g* for 15 min at 4 °C and the aqueous phase of the mixture was carefully

472 recovered and transferred to a fresh RNAse-free tube. RNA was precipitated with 500 µl of
473 cold isopropanol at room temperature for 10 min and then centrifuged at 12,000 x *g* for 15 min
474 at 4°C. The supernatant was carefully removed, the pellet was washed and vortexed with 1 ml
475 of 75% ethanol and centrifuged at 7,500 x *g* for 5 min at 4°C. RNA pellet was air-dried,
476 dissolved in the appropriate volume of DEPC-treated water and the concentration, 260/280 and
477 260/230 ratios were measured by Nanodrop. RNA integrity was evaluated in the Agilent 2200
478 Tapestation system.
479
480 **RNA mass spectrometry**
481 Up to 10 µg of RNA was digested by adding 1 µl digestion enzyme mix per well in a digestion
482 buffer (4 mM Tris-HCl pH 8, 5 mM MgCl2, 20 mM NaCl) in a total volume of up to 100 µl.
483 The digestion enzyme mix was made by mixing benzonase (250 U/µl, Sigma Aldrich),
484 phosphodiesterase I from *Crotalus adamanteus* venom (10mU/µl, Sigma Aldrich) and
485 Antarctic phosphatase (5 U/µl, NEB) in a ratio of 1:10:20. The reaction was incubated
486 overnight at 37 °C. The following day, an equal volume of $^{13}C$, $^{15}N$-labelled uridine (internal
487 control, previously dephosphorylated; Sigma Aldrich) in 0.1% formic acid was added to each
488 reaction and this was subsequently prepared for LC-MS-MS by filtration through 30 kDa
489 molecular weight cut-o filters (Sigma).
490 Samples were resolved using a Thermo Scientific U3000 UPLC system on a gradient
491 of 2- 98% (0.1% formic acid/acetonitrile) through an Acquity 100mm x 2.1 mm C-18 HSS T3
492 column and analysed on a QExactive-HF Orbitrap High Resolution Mass Spectrometer
493 (ThermoFisher Scientific, IQLAAEGAAPFALGMBFZ) in positive full-scan mode and the
494 results were deconvoluted using the accompanying Xcalibur Software. Nucleosides of interest
495 were identified by both retention times and accurate masses, compared to purified standards
496 and quantified accordingly.
497
498 **Whole Transcriptome Bisulfite Sequencing**
499 Bisulfite sequencing experiments were performed as previously described in Legrand *et al*
500 (Legrand *et al*, 2017). RNA was fractionated into <200 nt and >200 nt using a modified
501 mirVana miRNA isolation kit (AM1560) protocol. Briefly, 50 µg of RNA in a volume of 80
502 µl were mixed with 400 µl of mirVana lysis/binding buffer and 48 µl of mirVana homogenate
503 buffer and incubated for 5 min at room temperature. Next, 1/3 volume (176 µl) of 100% ethanol
504 was added and thoroughly mixed by inversion, and the mixture was incubated for 20 min at
505 room temperature. After addition of 0.8 µg of Glycoblue, the samples were spun down at 2,500

506 x g for 8 min at 21 °C for precipitation of long RNAs. The supernatant containing the short
507 fraction was transferred to a fresh tube and the RNA pellet was washed in 1 ml of cold 75%
508 ethanol before centrifugation at maximum speed for at least 20 min at 4 °C. The pellet was
509 finally air-dried and resuspended in DEPC-treated water. For short fraction RNA precipitation,
510 800 µl of isopropanol were added to the supernatant and the mixture was incubated at -80 °C
511 for at least 20 min. Next, 20 µg of Glycoblue were added and the mixture was spun down at
512 maximum speed for at least 20 min at 4 °C. The pellet was washed with cold 70% ethanol and
513 air dried before resuspension in DEPC-treated water. Depletion of ribosomal RNA was
514 performed on the short fractions and on half of the long fractions using a Ribo-zero rRNA
515 removal kit (Illumina), according to the supplier's instructions. The other half of long fractions
516 was processed as Ribo+ samples. RNA was stored at -80 °C until the moment of use.
517 The long fractions (with and without rRNA depletion) were further processed with the
518 NEBNext Magnesium RNA Fragmentation Module (NEB), as described in the manual. 3 min
519 of fragmentation at 94 °C has been established to lead to a peak at approximately 250 nt,
520 appropriate for the final 100 bp paired-end sequencing. The fragmented RNA was precipitated
521 using ethanol with 20 µg GlycoBlue at -80 °C for at least 10 min.
522 Samples were treated with TURBO DNase (Ambion) in a final volume of 20 µl,
523 according to the manufacturer's instructions. DNase-treated samples were bisulfite-converted
524 using an EZ RNA Methylation Kit (Zymo Research), following the manufacturer's manual. As
525 a final step before library preparation, a stepwise RNA end repair was carried out using T4
526 polynucleotide kinase (TaKaRa). A 3′-dephosphorylation and 5′- phosphorylation reaction was
527 performed using T4 PNK enzyme (TaKaRa). The enzyme was removed by phenol-chloroform
528 purification. Library preparation was done using a NEBNext Small RNA Library Prep Set,
529 according to the manufacturer's protocol. cDNA was amplified with 12 cycles of PCR and
530 purified using the QIAquick PCR Purification Kit (Qiagen). The libraries were size-selected
531 on a 6% polyacrylamide gel. Compatible barcodes were selected, and samples were pooled in
532 equimolar ratios on multiple lanes in an Illumina HiSeq 2000 platform. A 100 bp paired-end
533 sequencing approach was used.
534 Bioinformatics, statistical analyses and methylation calling were performed as
535 described in Legrand *et al* (Legrand *et al*, 2017), utilising the BisRNA software. Adapters were
536 removed from sequenced reads using Cutadapt version 1.8.1 (with options: --error-rate=0.1 --
537 times=2 --overlap=1 and adapter sequences AGATCGGAAGAGCACACGTCT and
538 GATCGTCGGACTGTAGAACTCTGAAC for forward and reverse reads, respectively
539 (Martin, 2011). Reads were further trimmed of bases with phred quality score <30 on 5' and 3'

540 ends and reads shorter than 25 nucleotides were discarded (Trimmomatic version 0.36)
541 (Bolger, Lohse, & Usadel, 2014). Reads were aligned uniquely using Bsmap (version 2.87,
542 options: -s 12 -v 0.03 -g 0 -w 1000 -S 0 -p 1 -V 1 -I 1 -n 0 -r 2 -u -m 15 -x 1000) (Xi & Li,
543 2009). Reference sequences were downloaded from Gtrnadb (version ce10), Ensembl (release
544 90, version WBcel235) and Arb-Silva (P. P. Chan & Lowe, 2016; Kersey *et al*, 2016; Lee *et*
545 *al*, 2018; Quast *et al*, 2012). End sequence 'CCA' was appended to tRNA if missing. Bisulfite-
546 identical sequences, where only C>T point differences were present, were merged, keeping the
547 C polymorphism. Similarly to Legrand *et al* (Legrand *et al*, 2017), tRNA sequences were
548 further summarized to the most exhaustive yet unambiguous set of sequences, using sequence
549 similarity matrix from Clustal Omega (Sievers *et al*, 2011). Methylation calling was performed
550 as described in Legrand *et al* (Legrand *et al*, 2017), utilising the BisRNA software. Methylation
551 frequency was calculated as the proportion of cytosines with coverage higher than 10 in three
552 wild type and noNSUN replicates and bisulfite non-conversion ratio higher than 0.1. The
553 measure for reproducibility was the standard error. Deamination rates were calculated as the
554 count of converted cytosines divided by the sum of converted and non-converted cytosines.
555 This calculation was carried out on nuclear and mitochondrial rRNA. Known methylation sites
556 in rRNA were removed from the calculations. WTBS raw data have been deposited in the Gene
557 Expression Omnibus (GEO) database under the accession number GSE144822.
558
559 **Targeted bisulfite sequencing**
560 1 µg of total RNA was bisulfite-modified with the EZ RNA Methylation Kit (Zymo Research).
561 Briefly, samples were first treated with DNase I for 30 min at 37 °C in 20 µl volume. The
562 DNAse reaction was stopped and immediately applied to the EZ RNA Methylation Kit (Zymo
563 Research) according to manufacturer's instructions. Converted RNAs were eluted in 12 µl of
564 distilled water.
565 Reverse transcription was performed with the purified RNA and adaptors were added
566 to the amplicons using reverse oligonucleotides designed for the bisulfite-converted sequences
567 of interest and SuperScript III reverse transcriptase (Invitrogen). cDNA was cleaned from any
568 residual RNA with an RNase H treatment at 37 °C for 20 min and then used for PCR
569 amplification and adaptor addition using forward oligonucleotides. Low annealing temperature
570 (58 °C) was used to overcome high A-T content after bisulfite treatment. 4 µl of PCR product
571 were used for ligation and transformation into TOP10 competent cells using the Zero Blunt
572 TOPO PCR Cloning Kit (Invitrogen) according to the manufacturer's instructions. Following
573 overnight culture, 24 colonies were individually lysed and used for PCR amplification using

M13 primers, in order to confirm the presence of the insert at the correct size by DNA electrophoresis. The remaining PCR product (10 clones per condition) was used for Sanger sequencing using T3 primers (Genewiz).

## Automated phenotypical characterisation

### Viable Progeny

Viable progeny refers to the number of progeny able to reach at least the L4 stage within ~4 days. Measurements were completed over three 24-h intervals. First, eggs were prepared by synchronisation via coordinated egg-laying. When these animals had grown to the L4 stage, single animals were transferred to fresh plates (day 0). For 3 days, each day (days 1–3), each animal was transferred to a new plate, while the eggs were left on the old plate and allowed to hatch and grow for ~ 3 days, after which, the number of animals on each of these plates was counted (Hodgkin & Barnes, 1991) using a custom animal counting program utilising short video recordings. Animals were agitated by tapping each plate four times, after this, 15 frames were imaged at 1 Hz and the maximum projection was used as a background image. Animals were then detected by movement using the difference in the image between each frame and this background image and counted this way for ten additional frames. The final count was returned as the mode of these counts. This system was tested on plates with fixed numbers of animals and was accurate to within 5%, comparable to human precision. Total viable progeny was reported then as the sum for 3 days. Data is censored for animals that crawled off of plates (Akay *et al*, 2019).

### Single Worm Growth Curves

Populations of *Caenorhabditis elegans* were synchronized by coordinated egg laying. Single eggs were transferred to individual wells of a multi-well NGM plate solidified with Gelrite (Sigma). Each well was inoculated with 1 $\mu l$ of OD 20 *E. coli* HB101 bacteria (~18 million) and imaged periodically using a camera mounted to a computer controlled XY plotter (EleksMaker, Jiangsu, China) which moved the camera between different wells. Images were captured every ~11 minutes for ~75 hours. Image processing was done in real-time using custom MATLAB scripts, storing both properties of objects identified as *C. elegans*, and sub images of regions around detected objects. Body length was calculated using a custom MATLAB (Mathworks, Natick MA) algorithm and all other properties were measured using the *regionprops* function. Growth curves were aligned to egg-hatching time, which was manually determined for each animal.

608

609 **Polysome profiling**

610 Synchronised populations of the strains of interest (N2 and noNSUN) were grown until adult
611 stage (3 days) in 140 mm NGM agar plates seeded with concentrated *E. coli* HB101 cultures
612 at 20 °C. Next, the animals were harvested from the plates, transferred to liquid cultures in S-
613 medium supplemented with *E. coli* HB101, and incubated at 20°C or 27°C for 4h in a shaking
614 incubator at 200 rpm before harvesting. Sample preparation for polysome profiling was
615 adapted from Arnold et al (Arnold *et al*, 2014). The animals were harvested, washed 3x in cold
616 M9 buffer supplemented with 1 mM cycloheximide and once in lysis buffer (20 mM Tris pH
617 8.5, 140 mM KCl, 1.5 mM MgCl2, 0.5% Nonidet P40, 2% PTE (polyoxyethylene-10-
618 tridecylether), 1% DOC (sodiumdeoxycholate monohydrate), 1 mM DTT, 1 mM
619 cycloheximide). The animals were pelleted and as much liquid as possible was removed before
620 the samples were frozen as droplets in liquid nitrogen, using a Pasteur pipette. Frozen droplets
621 were transferred to metallic capsules and cryogenically ground for 25 sec in a mixer (Retsch
622 MM 400 Mixer Mill). The resulting frozen powder was stored at -80 °C until the moment of
623 use.

624 Approximately 250 µl of frozen powder was added to 600 µl of lysis buffer and mixed
625 by gentle rotation for 5 min at 4 °C. The samples were centrifuged at 10,000 x g for 7.5 min,
626 the supernatant was transferred to fresh tubes and the RNA concentration was quantified by
627 Nanodrop. For ribosome footprinting, 400 µl of lysate was treated with 4 µl of DNase I (1 U/µl,
628 Thermo Scientific) and 8 µl of RNase I (100 U/µl, Ambion) for 45 min at room temperature
629 with gentle shaking. 20 µl of RNasin ribonuclease inhibitor (40 U/µl, Promega) was added to
630 quench the reaction when appropriate. The tubes were immediately put on ice and 220 µl of
631 lysate was loaded into 17.5 – 50% sucrose gradients and ultracentrifuged for 2.5 h at 35,000
632 rpm, 4 °C in a Beckman SW60 rotor. In parallel, undigested samples used for polysome
633 profiling were equally loaded into sucrose gradients under the same conditions. Gradient
634 fractions were eluted with an ISCO UA-6 gradient fractionator while the absorbance at 254 nm
635 was continuously monitored. The fraction of polysomes engaged in translation was calculated
636 as the area under the polysomal part of the curve divided by the area below the entire curve.

637

638 **Ribosome profiling**

639 Sucrose gradient fractions were collected in tubes containing 300 µl of 1 M Tris-HCl pH 7.5,
640 5M NaCl, 0.5 M EDTA, 10% SDS, 42% urea and then mixed by vortexing with 300 µl of
641 Phenol-Chloroform-Isoamylalcohol (PCL, 24:25:1). Fractions corresponding to 80S

642 monosomes were heated for 10 min at 65°C and centrifuged at 16,000 x g for 20 min at room
643 temperature. The upper aqueous phase was transferred to a fresh tube and mixed well with
644 600 µl of isopropanol and 1 µl of Glycoblue for precipitation overnight at -80 °C. RNA was
645 pelleted by centrifugation at 16,000 x g for 20 min at 4 °C and washed in 800 µl of cold ethanol.
646 After supernatant removal, the pellet was left to dry for 1-2 min and then dissolved in 60 µl of
647 RNase-free water. RNA concentration and quality were measured by Nanodrop and
648 Tapestation (2200 Agilent R6K), respectively.

649 A dephosphorylation reaction was performed by adding 7.5 µl T4 polynucleotide kinase
650 (PNK) 10x buffer, 1.5 µl ATP, 1.5 µl RNase OUT, 1.5 µl T4 PNK (TaKaRa) and 3 µl RNase-
651 free water up to a final volume of 75 µl, and incubated for 1.5 h at 37 °C. The enzyme was
652 removed by acid-phenol extraction and the RNA was precipitated with 1/10 volume 3 M
653 sodium acetate pH 5.2, 2.5x volume 100% cold ethanol and 1 µl Glycoblue overnight at -80°C.
654 Pelleted RNA was dissolved in RNase-free water. For footprint fragments purification, RNA
655 was denaturated for 3 min at 70 °C and loaded into a 15% polyacrylamide TBE-urea gel
656 alongside a small RNA marker. Gel was run for 1 h at 150 V and stained for 10 min with
657 1:10,000 SYBR Gold in 0.5x TBE. The gel was visualised under UV light and the region
658 between the 20 nt and 30 nt marks (28-32 nt) was excised with a sterile scalpel. The gel band
659 was crushed into small pieces and incubated in 300 µl of 0.3 M RNase-free NaCl solution with
660 2 µl of RNase OUT overnight at 4°C on an Intelli-Mixer (Elmi). The gel slurry was transferred
661 to a 0.45 µm NanoSep MF Tube (Pall Lifesciences) and centrifuged at maximum speed for 5
662 min at 4°C. After overnight precipitation with 30 µl of 3 M sodium acetate pH 5.2, 1 µl
663 Glycoblue and 800 µl 100% ethanol, the RNA was dissolved in RNase-free water.

664 Libraries were prepared using a NEB NEXT Small RNA Library Prep Set for Illumina
665 (Multiplex compatible) E7330 Kit, following the manufacturer's instructions. cDNA libraries
666 were purified according to the manual, followed by a QIAQuick PCR Purification Kit and a
667 6% polyacrylamide gel, where a band of 150 bp (120 bp adapter + 28-32 footprint fragments)
668 was excised. Gel extraction was performed as described above for footprint fragments
669 purification. Libraries were sequenced at the Genomics and Proteomics Core Facility of the
670 German Cancer Research Centre (DKFZ), Heidelberg.

671 Raw reads were assessed for quality using FastQC and Trimmed for low quality bases
672 and adapter sequences using Trimmomatic (version 0.39, parameters -
673 ILLUMINACLIP:2:30:10 SLIDINGWINDOW:4:20 MINLEN:20) (Bolger *et al*, 2014).
674 SortMERNA was used to remove any rRNA sequences (Kopylova, Noé, & Touzet, 2012).
675 Remaining reads were uniquely aligned to the *C. elegans* (WBCel235) reference genome using

676 HISAT2 (version 2.1.0) (Kim *et al*, 2015). The longest transcript was chosen for each gene
677 from the WBCel235 reference genome and the CDS for these transcripts was extracted. Reads
678 were length stratified and checked for periodicity, only read lengths showing periodicity over
679 the 3 frames were retained for further analysis (26 bp -30 bp). Reads aligned to the genome
680 were shifted 12 bp from the 5′-end towards the 3′-end (Ingolia *et al*, 2009)i. Any reads aligned
681 to the first 10 codons of each gene were then removed and the remaining reads with a 5′ end
682 aligning to a CDS were kept for further analysis (Lecanda *et al*, 2016).
683 Bulk codon occupancy in the P-Site for each codon was calculated as the number of
684 shifted RPFs assigned to the first nucleotide of the codon. This value was then normalized by
685 the frequency of the counts for the same codon in the +1, +2 and +3 codons relative to the A-
686 Site (Stadler & Fire, 2011). Fold changes were then computed as the normalized bulk codon
687 occupancies for noNSUN / wild type. Ribosome occupancy for gene in a sample was calculated
688 as the number of shifted in frame RPFs aligned to the CDS of the gene (not including the first
689 10 codons). These values were inputted into DESeq2 (Love *et al*, 2014). Translation efficiency
690 was calculated by dividing the ribosome occupancy of each gene (disregarding the first ten
691 codons) by the mRNA abundance of the same gene. Ribo-Seq raw data have been deposited in
692 the Gene Expression Omnibus (GEO) database under the accession number GSE146256.
693
694 **RNA sequencing**
695 Input RNA was extracted from aliquots from the samples used for polysome profiling and
696 ribosome footprinting. 100 µl of chloroform were added to the tubes, which were then shaken
697 vigorously for 15 sec and incubated at room temperature for 3 min. Samples were centrifuged
698 at 12,000 x g for 15 min at 4 °C and the aqueous phase of the mixture was carefully recovered
699 and transferred to a fresh RNAse-free tube. RNA was precipitated with 500 µl of cold
700 isopropanol at room temperature for 10 min and then centrifuged at 12,000 x g for 15 min at
701 4 °C. The supernatant was carefully removed, the pellet was washed and vortexed with 1 ml of
702 75% ethanol and centrifuged at 7,500 x g for 5 min at 4°C. RNA pellet was air-dried, dissolved
703 in the appropriate volume of DEPC-treated water and the concentration, 260/280 and 260/230
704 ratios were measured by Nanodrop. RNA integrity was evaluated in the Agilent 2200
705 Tapestation system. RNA was depleted of DNA with a TURBO DNA-free kit (Invitrogen),
706 according to the manufacturer's instructions. Libraries were prepared with 750 ng of starting
707 material using the NEBNext Ultra II Directional RNA Library Prep Kit for Illumina, following
708 rRNA depletion using a NEBNext rRNA Depletion Kit (Human/Mouse/Rat) (NEB).

Raw reads were assessed for quality using FastQC (Andrews, 2010) and Trimmed for low quality bases and adapter sequences using Trimmomatic (version 0.39, parameters - ILLUMINACLIP:2:30:10 SLIDINGWINDOW:4:20 MINLEN:25) (Bolger *et al*, 2014). SortMERNA (Kopylova *et al*, 2012) was used to remove any reads matching rRNA sequences. Remaining reads were aligned to the *C. elegans* reference genome (WBCel235) using HISAT2 (version 2.1.0, default parameters) (Kim *et al*, 2015). Read alignments were then counted using HTSeq-count (Anders *et al*, 2015) and gene counts inputted into DESeq2 (Love *et al*, 2014). RNA-Seq raw data have been deposited in the Gene Expression Omnibus (GEO) database under the accession number GSE146256.

**Data availability**

BS-seq: Gene Expression Omnibus (GEO) GSE144822
(https://www.ncbi.nlm.nih.gov/geo/query/acc.cgi?acc=GSE144822)
RNA-seq: Gene Expression Omnibus (GEO) GSE146256
(https://www.ncbi.nlm.nih.gov/geo/query/acc.cgi?acc=GSE146256)
Ribo-seq: Gene Expression Omnibus (GEO) GSE146256
(https://www.ncbi.nlm.nih.gov/geo/query/acc.cgi?acc=GSE146256)

**ACKNOWLEDGEMENTS**

We would like to thank the Gurdon Institute Media Kitchen for their support providing reagents and media. We thank Kay Harnish for the Gurdon Institute Sequencing Facility management. We thank Julie Ahringer's lab for kindly sharing RNAi bacterial clones. We thank the National Bioresource Project (Tokyo, Japan) for providing the *nsun-5* deletion allele. We thank Claudia Flandoli for illustrating our working model. We thank Archana Yerra for manuscript editing. We are grateful to the Miska Laboratory members, especially Kin Man Suen, Eyal Maori, Ragini Medhi and Grégoire Vernaz, for helpful discussions and advice. We are grateful to Miranda Landgraf for her constant support, and to Marc Ridyard for laboratory management and maintenance of our nematode collection. This research was supported by a Wellcome Trust Senior Investigator award (104640/Z/14/Z) and Cancer Research UK award (C13474/A27826) to E.A.M ; Conselho Nacional de Desenvolvimento Científico e Tecnológico doctorate scholarship (CNPq, Brazil - 205589/2014-6) to I.C.N.; Deutsche Forschungsgemeinschaft

742 (SPP1784) to F.L. The Miska Laboratory was also supported by core funding from the
743 Wellcome Trust (092096/Z/10/Z, 203144/Z/16/Z) and Cancer Research UK (C6946/A24843).
744
745
746 **AUTHOR CONTRIBUTIONS**
747 Conceptualisation, I.C.N. and E.A.M.; Investigation, I.C.N., F.T., D.J., A.H., F.B., A.K. and
748 A.A.; Formal analysis, D.J., C.L. and J.P.; Writing - Original Draft, I.C.N.; Writing - Review
749 and Editing, I.C.N., F.T., A.A., F.L. and E.A.M.; Supervision: M.H., F.L. and E.A.M.; Funding
750 Acquisition, M.H., F.L. and E.A.M.
751
752
753 **COMPETING INTERESTS**
754 E.A.M. is a co-founder and director of Storm Therapeutics, Cambridge, UK. A.H. is an
755 employee of Storm Therapeutics, Cambridge, UK.
756
757
758 **REFERENCES**
759
760 Abbasi-Moheb L, Mertel S, Gonsior M, Nouri-Vahid L, Kahrizi K, Cirak S, Wieczorek D,
761 Motazacker MM, Esmaeeli-Nieh S, Cremer K, *et al* (2012) Mutations in NSUN2 cause
762 autosomal- Recessive intellectual disability. *Am J Hum Genet* 90: 847–855
763 Adams JM & Cory S (1975) Modified nucleosides and bizarre 5′-termini in mouse myeloma
764 mRNA. *Nature* 255: 28–33
765 Akay A, Jordan D, Navarro IC, Wrzesinski T, Ponting CP, Miska EA & Haerty W (2019)
766 Identification of functional long non-coding RNAs in C. elegans. *BMC Biol* 17: 14
767 Amort T, Rieder D, Wille A, Khokhlova-Cubberley D, Riml C, Trixl L, Jia X-Y, Micura R &
768 Lusser A (2017) Distinct 5-methylcytosine profiles in poly(A) RNA from mouse
769 embryonic stem cells and brain. *Genome Biol* 18: 1
770 Anders S, Pyl PT & Huber W (2015) HTSeq-A Python framework to work with high-
771 throughput sequencing data. *Bioinformatics* 31: 166–169
772 Arnold A, Rahman MM, Lee MC, Muehlhaeusser S, Katic I, Gaidatzis D, Hess D, Scheckel
773 C, Wright JE, Stetak A, *et al* (2014) Functional characterization of C. elegans Y-box-
774 binding proteins reveals tissue-specific functions and a critical role in the formation of
775 polysomes. *Nucleic Acids Res* 42: 13353–13369

776 De Beus E, Brockenbrough JS, Hong B & Aris JP (1994) Yeast NOP2 encodes an essential
777 nucleolar protein with homology to a human proliferation marker. *J Cell Biol* 127:
778 1799–1813
779 Blanco S, Bandiera R, Popis M, Hussain S, Lombard P, Aleksic J, Sajini A, Tanna H, Cortés-
780 Garrido R, Gkatza N, *et al* (2016) Stem cell function and stress response are controlled
781 by protein synthesis. *Nature* 534: 335–340
782 Blanco S, Dietmann S, Flores J V, Hussain S, Kutter C, Humphreys P, Lukk M, Lombard P,
783 Treps L, Popis M, *et al* (2014) Aberrant methylation of tRNAs links cellular stress to
784 neuro-developmental disorders. *EMBO J* 33: 1–20
785 Boccaletto P, Machnicka MA, Purta E, Pi¸ Atkowski P-L, Zej Bagí Nski B-L, Wirecki TK,
786 De Crécy V, Crécy-Lagard C, Ross R, Limbach PA, *et al* (2017) MODOMICS: a
787 database of RNA modification pathways. 2017 update. *Nucleic Acids Res* 46: 303–307
788 Bolger AM, Lohse M & Usadel B (2014) Trimmomatic: a flexible trimmer for Illumina
789 sequence data. *Bioinformatics* 30: 2114–2120
790 Brenner S (1974) The genetics of Caenorhabditis elegans. *Genetics* 77: 71–94
791 Burgess AL, David R & Searle IR (2015) Conservation of tRNA and rRNA 5-methylcytosine
792 in the kingdom Plantae. *BMC Plant Biol* 15: 1–17
793 Chan CTY, Dyavaiah M, DeMott MS, Taghizadeh K, Dedon PC & Begley TJ (2010) A
794 Quantitative Systems Approach Reveals Dynamic Control of tRNA Modifications
795 during Cellular Stress. *PLoS Genet* 6: e1001247
796 Chan CTY, Pang YLJ, Deng W, Babu IR, Dyavaiah M, Begley TJ & Dedon PC (2012)
797 Reprogramming of tRNA modifications controls the oxidative stress response by codon-
798 biased translation of proteins. *Nat Commun* 3
799 Chen X, Li A, Sun B-F, Yang Y, Han Y-N, Yuan X, Chen R-X, Wei W-S, Liu Y, Gao C-C,
800 *et al* (2019) 5-methylcytosine promotes pathogenesis of bladder cancer through
801 stabilizing mRNAs. *Nat Cell Biol* 21: 978–990
802 David R, Burgess A, Parker B, Li J, Pulsford K, Sibbritt T, Preiss T & Searle IR (2017)
803 Transcriptome-wide Mapping of RNA 5-Methylcytosine in Arabidopsis mRNAs and
804 non-coding RNAs. *Plant Cell*: tpc.00751.2016
805 van Delft P, Akay A, Huber SM, Bueschl C, Rudolph KLM, Di Domenico T, Schuhmacher
806 R, Miska EA & Balasubramanian S (2017) The Profile and Dynamics of RNA
807 Modifications in Animals. *Chembiochem* 18: 979–984
808 Desrosiers, Ronald Friderici, Karen Rottman F (1974) Identification of Methylated
809 Nucleosides in Messenger RNA from Novikoff Hepatoma Cells. *Proc Natl Acad Sci* 71:

810 3971–3975
811 Edelheit S, Schwartz S, Mumbach MR, Wurtzel O & Sorek R (2013) Transcriptome-Wide
812 Mapping of 5-methylcytidine RNA Modifications in Bacteria, Archaea, and Yeast
813 Reveals m5C within Archaeal mRNAs. *PLoS Genet* 9: e1003602
814 Flores J V., Cordero-Espinoza L, Oeztuerk-Winder F, Andersson-Rolf A, Selmi T, Blanco S,
815 Tailor J, Dietmann S & Frye M (2016) Cytosine-5 RNA Methylation Regulates Neural
816 Stem Cell Differentiation and Motility. *Stem Cell Reports* 8
817 García-Vílchez R, Sevilla A & Blanco S (2019) Post-transcriptional regulation by cytosine-5
818 methylation of RNA. *Biochim Biophys Acta - Gene Regul Mech*: #pagerange#
819 Goll MG, Kirpekar F, Maggert KA, Yoder JA, Hsieh C, Zhang X, Golic KG, Jacobsen SE &
820 Bestor TH (2006) Methylation of tRNA Asp by the DNA Methyltransferase Homolog
821 Dnmt2. *Science* 311: 395–398
822 Haag S, Sloan KE, Ranjan N, Warda AS, Kretschmer J, Blessing C, Hübner B, Seikowski J,
823 Dennerlein S, Rehling P, *et al* (2016) NSUN3 and ABH1 modify the wobble position of
824 mt-tRNAMet to expand codon recognition in mitochondrial translation. *Embo J* 35:
825 DOI: 10.15252/embj.201694885
826 Haag S, Warda AS, Kretschmer J, Günnigmann MA, Höbartner C & Bohnsack MT (2015)
827 NSUN6 is a human RNA methyltransferase that catalyzes formation of m5C72 in
828 specific tRNAs. *RNA*: rna.051524.115-
829 Van Haute L, Dietmann S, Kremer L, Hussain S, Pearce SF, Powell CA, Rorbach J, Lantaff
830 R, Blanco S, Sauer S, *et al* (2016) Deficient methylation and formylation of mt-
831 tRNAMet wobble cytosine in a patient carrying mutations in NSUN3. *Nat Commun* 7:
832 12039
833 Heissenberger C, Krammer TL, Rollins JA, Nagelreiter F, Stocker I, Wacheul L, Shpylovyi
834 A, Snow S, Rogers AN, Lafontaine DL, *et al* (2020) The ribosomal RNA m5C
835 methyltransferase NSUN-1 modulates healthspan and oogenesis in Caenorhabditis
836 elegans. bioRxiv doi: 10.1101/2020.03.16.993469 [PREPRINT]
837 Heissenberger C, Liendl L, Nagelreiter F, Gonskikh Y, Yang G, Stelzer EM, Krammer TL,
838 Micutkova L, Vogt S, Kreil DP, *et al* (2019) Loss of the ribosomal RNA
839 methyltransferase NSUN5 impairs global protein synthesis and normal growth. *Nucleic*
840 *Acids Res* 47: 11807–11825
841 Hodgkin J & Barnes TM (1991) More is not better: Brood size and population growth in a
842 self-fertilizing nematode. *Proc R Soc B Biol Sci* 246: 19–24
843 Hong B, Brockenbrough JS, Wu P & Aris JP (1997) Nop2p is required for pre-rRNA

844 processing and 60S ribosome subunit synthesis in yeast. *Mol Cell Biol* 17: 378–388
845 Hong B, Wu K, Brockenbrough JS, Wu P & Aris JP (2001) Temperature sensitive nop2
846 alleles defective in synthesis of 25S rRNA and large ribosomal subunits in
847 Saccharomyces cerevisiae. *Nucleic Acids Res* 29: 2927–37
848 Hopper AK & Phizicky EM (2003) tRNA transfers to the limelight. *Genes Dev* 17: 162–80
849 Huang T, Chen W, Liu J, Gu N & Zhang R (2019) Genome-wide identification of mRNA 5-
850 methylcytosine in mammals. *Nat Struct Mol Biol* 26: 380–388
851 Huber SM, van Delft P, Mendil L, Bachman M, Smollett K, Werner F, Miska E a. &
852 Balasubramanian S (2015) Formation and Abundance of 5-Hydroxymethylcytosine in
853 RNA. *ChemBioChem* 23: 752–755
854 Huber SM, Van Delft P, Tanpure A, Miska EA & Balasubramanian S (2017) 2′-O-methyl-5-
855 hydroxymethylcytidine: A second oxidative derivative of 5-methylcytidine in RNA. *J*
856 *Am Chem Soc* 139: 1766–1769
857 Ingolia NT, Ghaemmaghami S, Newman JRS & Weissman JS (2009) Genome-wide analysis
858 in vivo of translation with nucleotide resolution using ribosome profiling. *Science (80- )*
859 324: 218–223
860 Jackman JE & Alfonzo JD (2013) Transfer RNA modifications: Nature's combinatorial
861 chemistry playground. *Wiley Interdiscip Rev RNA* 4: 35–48
862 Kamath RS & Ahringer J (2003) Genome-wide RNAi screening in Caenorhabditis elegans.
863 *Methods* 30: 313–321
864 Kawarada L, Suzuki T, Ohira T, Hirata S, Miyauchi K & Suzuki T (2017) ALKBH1 is an
865 RNA dioxygenase responsible for cytoplasmic and mitochondrial tRNA modifications.
866 *Nucleic Acids Res* 45: 7401–7415
867 Khan MA, Rafiq MA, Noor A, Hussain S, Flores J V., Rupp V, Vincent AK, Malli R, Ali G,
868 Khan FS, *et al* (2012) Mutation in NSUN2, which encodes an RNA methyltransferase,
869 causes autosomal-recessive intellectual disability. *Am J Hum Genet* 90: 856–863
870 Khoddami V & Cairns BR (2013) Identification of direct targets and modified bases of RNA
871 cytosine methyltransferases. *Nat Biotechnol* 31: 458–464
872 Khoddami V, Yerra A, Mosbruger TL, Fleming AM, Burrows CJ & Cairns BR (2019)
873 Transcriptome-wide profiling of multiple RNA modifications simultaneously at single-
874 base resolution. *Proc Natl Acad Sci U S A* 116: 6784–6789
875 Khosronezhad N, Hosseinzadeh Colagar A & Mortazavi SM (2015) The Nsun7 (A11337)-
876 deletion mutation, causes reduction of its protein rate and associated with sperm motility
877 defect in infertile men. *J Assist Reprod Genet* 32: 807–815

878 Kim D, Langmead B & Salzberg SL (2015) HISAT: A fast spliced aligner with low memory
879 requirements. *Nat Methods* 12: 357–360
880 King MY & Redman KL (2002) RNA methyltransferases utilize two cysteine residues in the
881 formation of 5-methylcytosine. *Biochemistry* 41: 11218–11225
882 Komara M, Al-Shamsi AM, Ben-Salem S, Ali BR & Al-Gazali L (2015) A Novel Single-
883 Nucleotide Deletion (c.1020delA) in NSUN2 Causes Intellectual Disability in an
884 Emirati Child. *J Mol Neurosci* 57: 393–399
885 Kosi N, Alić I, Kolačević M, Vrsaljko N, Jovanov Milošević N, Sobol M, Philimonenko A,
886 Hozák P, Gajović S, Pochet R, *et al* (2015) Nop2 is expressed during proliferation of
887 neural stem cells and in adult mouse and human brain. *Brain Res* 1597: 65–76
888 Lafontaine D, Vandenhaute J & Tollervey D (1995) The 18s rRNA dimethvlase D i m l ~ is
889 required for pre-ribo ~ omal RNA processing in yeast. *Genes Dev*: 2470–2481
890 Lafontaine DL, Preiss T & Tollervey D (1998) Yeast 18S rRNA dimethylase Dim1p: a
891 quality control mechanism in ribosome synthesis? *Mol Cell Biol* 18: 2360–2370
892 Lecanda A, Nilges BS, Sharma P, Nedialkova DD, Schwarz J, Vaquerizas JM & Leidel SA
893 (2016) Dual randomization of oligonucleotides to reduce the bias in ribosome-profiling
894 libraries. *Methods* 107: 89–97
895 Legrand C, Tuorto F, Hartmann M, Liebers R, Jacob D, Helm M & Lyko F (2017)
896 Statistically robust methylation calling for wholetranscriptome bisulfite sequencing
897 reveals distinct methylation patterns for mouse RNAs. *Genome Res* 27: 1589–1596
898 Li J, Li H, Long T, Dong H, Wang E-D & Liu R-J (2018) Archaeal NSUN6 catalyzes m5C72
899 modification on a wide-range of specific tRNAs. *Nucleic Acids Res* 28: 2041–2055
900 Li Q, Li X, Tang H, Jiang B, Dou Y, Gorospe M & Wang W (2017) NSUN2-Mediated m5C
901 Methylation and METTL3/METTL14-Mediated m6A Methylation Cooperatively
902 Enhance p21 Translation. *J Cell Biochem* 118: 2587–2598
903 Liu Y & Santi D V (2000) m5C RNA and m5C DNA methyl transferases use different
904 cysteine residues as catalysts. *Proc Natl Acad Sci U S A* 97: 8263–8265
905 Long T, Li J, Li H, Zhou M, Zhou XL, Liu RJ & Wang ED (2016) Sequence-specific and
906 shape-selective RNA recognition by the human RNA 5-methylcytosine
907 methyltransferase NSun. *J Biol Chem* 291: 24293–24303
908 Love MI, Huber W & Anders S (2014) Moderated estimation of fold change and dispersion
909 for RNA-seq data with DESeq2. *Genome Biol* 15: 550
910 Lu ZJ, Yip KY, Wang G, Shou C, Hillier LDW, Khurana E, Agarwal A, Auerbach R,
911 Rozowsky J, Cheng C, *et al* (2011) Prediction and characterization of noncoding RNAs

912 in C. elegans by integrating conservation, secondary structure, and high-throughput
913 sequencing and array data. *Genome Res* 21: 276–285
914 Martinez FJ, Lee JH, Lee JE, Blanco S, Nickerson E, Gabrie S, Frye M, Al-Gazali L &
915 Gleeson JG (2012) Whole exome sequencing identifies a splicing mutation in NSUN2
916 as a cause of a Dubowitz-like syndrome. *J Med Genet* 49: 380–385
917 Metodiev MD, Spåhr H, Loguercio Polosa P, Meharg C, Becker C, Altmueller J, Habermann
918 B, Larsson NG & Ruzzenente B (2014) NSUN4 Is a Dual Function Mitochondrial
919 Protein Required for Both Methylation of 12S rRNA and Coordination of
920 Mitoribosomal Assembly. *PLoS Genet* 10: 1–11
921 Nakano S, Suzuki T, Kawarada L, Iwata H, Asano K & Suzuki T (2016) NSUN3 methylase
922 initiates 5-formylcytidine biogenesis in human mitochondrial tRNAMet. *Nat Chem Biol*
923 12: 546–551
924 O'Connor M, Leppik M & Remme J (2018) Pseudouridine-Free Escherichia coli Ribosomes.
925 *J Bacteriol* 200: e00540-17
926 Phizicky EM & Alfonzo JD (2010) Do all modifications benefit all tRNAs? *FEBS Lett* 584:
927 265–271
928 Ren HY, Zhong R, Ding XP, Chen ZY & Jing YL (2015) Investigation of polymorphisms in
929 exon7 of the NSUN7 gene among Chinese Han men with asthenospermia. *Genet Mol*
930 *Res* 14: 9261–9268
931 Salditt-Georgieff M, Jelinek W, Darnell JE, Furuichi Y, Morgan M & Shatkin A (1976)
932 Methyl labeling of HeLa cell hnRNA: a comparison with mRNA. *Cell* 7: 227–237
933 Schaefer M, Pollex T, Hanna K, Tuorto F, Meusburger M, Helm M & Lyko F (2010) RNA
934 methylation by Dnmt2 protects transfer RNAs against stress-induced cleavage. *Genes*
935 *Dev* 24: 1590–1595
936 Schosserer M, Minois N, Angerer TB, Amring M, Dellago H, Harreither E, Calle-Perez A,
937 Pircher A, Gerstl MP, Pfeifenberger S, *et al* (2015) Methylation of ribosomal RNA by
938 NSUN5 is a conserved mechanism modulating organismal lifespan. *Nat Commun* 6:
939 6158
940 Shanmugam R, Fierer J, Kaiser S, Helm M, Jurkowski TP & Jeltsch A (2015) Cytosine
941 methylation of tRNA-Asp by DNMT2 has a role in translation of proteins containing
942 poly-Asp sequences. *Cell Discov* 1: 1–10
943 Sharma S & Lafontaine DLJ (2015) 'View From A Bridge': A New Perspective on
944 Eukaryotic rRNA Base Modification. *Trends Biochem Sci* 40: 560–575
945 Sharma S, Yang J, Watzinger P, Kötter P & Entian KD (2013) Yeast Nop2 and Rcm1

946 methylate C2870 and C2278 of the 25S rRNA, respectively. *Nucleic Acids Res* 41:
947 9062–9076
948 Spåhr H, Habermann B, Gustafsson CM, Larsson N-G & Hallberg BM (2012) Structure of
949 the human MTERF4-NSUN4 protein complex that regulates mitochondrial ribosome
950 biogenesis. *Proc Natl Acad Sci U S A* 109: 15253–8
951 Squires JE, Patel HR, Nousch M, Sibbritt T, Humphreys DT, Parker BJ, Suter CM & Preiss T
952 (2012) Widespread occurrence of 5-methylcytosine in human coding and non-coding
953 RNA. *Nucleic Acids Res* 40: 5023–5033
954 Takemoto C, Spremulli LL, Benkowski LA, Ueda T, Yokogawa T & Watanabe K (2009)
955 Unconventional decoding of the AUA codon as methionine by mitochondrial tRNA Met
956 with the anticodon f 5 CAU as revealed with a mitochondrial in vitro translation system.
957 *Nucleic Acids Res* 37: 1616–1627
958 Tang H, Xiuqin Fan, Junyue Xing, Zhenyun Liu, Bin Jiang, Yali Dou, Gorospe M &
959 Wengong W (2015) NSun2 delays replicative senescence by repressing p27 (KIP1)
960 translation and elevating CDK1 translation. *Aging (Albany NY)* 7: 1143–58
961 Tuorto F, Herbst F, Alerasool N, Bender S, Popp O, Federico G, Reitter S, Liebers R,
962 Stoecklin G, Gröne H-J, *et al* (2015) The tRNA methyltransferase Dnmt2 is required for
963 accurate polypeptide synthesis during haematopoiesis. *Embo J* 34: 2350–62
964 Tuorto F, Liebers R, Musch T, Schaefer M, Hofmann S, Kellner S, Frye M, Helm M,
965 Stoecklin G & Lyko F (2012) RNA cytosine methylation by Dnmt2 and NSun2
966 promotes tRNA stability and protein synthesis. *Nat Struct Mol Biol* 19: 900–905
967 Wagner A, Hofmeister O, Rolland SG, Maiser A, Aasumets K, Schmitt S, Schorpp K,
968 Feuchtinger A, Hadian K, Schneider S, *et al* (2019) Mitochondrial Alkbh1 localizes to
969 mtRNA granules and its knockdown induces the mitochondrial UPR in humans and C.
970 elegans.
971 Watanabe Y, Tsuruis H, Ueda T, Furushimag R, Takamiyas S, Kitan K, Nishikawall K &
972 Watanabe K (1994) Primary and Higher Order Structures of Nematode (Ascaris suum)
973 Mitochondrial tRNAs Lacking Either the T or D Stem*. *J Biol Chem* 269: 22902–22906
974 Xiao T, Wang Y, Luo H, Liu L, Wei G, Chen X, Sun Y, Chen X, Skogerbø G & Chen R
975 (2012) A differential sequencing-based analysis of the C. elegans noncoding
976 transcriptome. *Rna* 18: 626–639
977 Yakubovskaya E, Guja KE, Mejia E, Castano S, Hambardjieva E, Choi WS & Garcia-Diaz M
978 (2012) Structure of the essential MTERF4:NSUN4 protein complex reveals how an
979 MTERF protein collaborates to facilitate rRNA modification. *Structure* 20: 1940–1947

980 Yang X, Yang Y, Sun B-F, Chen Y-S, Xu J-W, Lai W-Y, Li A, Wang X, Bhattarai DP, Xiao
981 W, *et al* (2017) 5-methylcytosine promotes mRNA export — NSUN2 as the
982 methyltransferase and ALYREF as an m5C reader. *Cell Res* 27: 606–625
983 Zhang X, Liu Z, Yi J, Tang H, Xing J, Yu M, Tong T, Shang Y, Gorospe M & Wang W
984 (2012) The tRNA methyltransferase NSun2 stabilizes p16INK4 mRNA by methylating
985 the 3′-untranslated region of p16. *Nat Commun* 3: 712
986 Zorbas C, Nicolas E, Wacheul L, Huvelle E, Heurgue-Hamard V & Lafontaine DL (2015)
987 The human 18S rRNA base methyltransferases DIMT1L and WBSCR22-TRMT112 but
988 not rRNA modification are required for ribosome biogenesis. *Mol Biol Cell*
989
990
991 **FIGURE LEGENDS**
992
993 **Figure 1. $m^5C$ and its derivatives are non-essential RNA modifications in *C. elegans*.**
994 **(A)** Phylogenetic relationship among human and putative nematode NSUN proteins. Unrooted
995 phylogenetic tree of NSUN homologues in *Homo sapiens* and *C. elegans* using entire protein
996 sequence. Phylogenetic tree reconstructed using the maximum likelihood method implemented
997 in the PhyML program (v3.0).
998 **(B, C)** Knockdown of *nsun* genes through RNAi by feeding. Representative images of wild
999 type adult animals after silencing of *nsun* genes via RNAi by feeding. Widefield DIC images
1000 are 10x magnification (B). Percentage of fertile adults after gene silencing by RNAi (C). n = 2
1001 independent experiments, 3 biological replicates each.
1002 **(D)** Mutant alleles used in this study. CRISPR-Cas9 strategy for creation and screening of
1003 catalytically inactive alleles of *nsun-1* (*mj473*), *nsun-2* (*mj458*) and *nsun-4* (*mj457*). A
1004 homologous recombination template bearing a point mutation to convert the catalytic cysteine
1005 into alanine whilst creating a restriction site for HaeIII was co-injected. For the study of *nsun-*
1006 *5*, a 928 bp deletion allele (*tm3898*) was used. Image not to scale.
1007 **(E, F)** Mass spectrometry quantification of $m^5C$ (D) and $hm^5Cm$ (E) levels in total RNA from
1008 *nsun* mutants. RNA was extracted from populations of L1 animals synchronised by starvation,
1009 digested to nucleosides and analysed via LC-MS. n = 3 independent biological replicates. n.d.
1010 = not detected.
1011 **(G)** Fold change in total RNA modification levels upon loss of $m^5C$. Fold changes were
1012 calculated by dividing the peak area ratio of noNSUN samples by the one of wild type samples.
1013 n = 3 independent biological replicates. Multiple t-tests.

1014 Data information: In (C, E, F, G), data are presented as mean ± SEM. In (C), a representative
1015 plot of two independent experiments is shown.
1016

1017 **Figure 2. The $m^5C$ methylome of *C. elegans*.**

1018 **(A, B)** Site-specific methylation analysis by whole-transcriptome bisulfite sequencing. Scatter
1019 plots show individual cytosines and their respective non-conversion rates in rRNAs (A) and
1020 tRNAs (B) of wild type and noNSUN strains; pie chart showing most frequently methylated
1021 tRNA isoacceptors.

1022 **(C)** Heatmap showing non-conversion rates of tRNA positions methylated in stoichiometry
1023 higher than 50% and of tRNA positions predicted to be targets of DNMT2 and NSUN6.

1024 **(D)** Site-specific methylation analysis by whole-transcriptome bisulfite sequencing. Scatter
1025 plot shows density of cytosines and their respective non-conversion rates in mRNAs of wild
1026 type and noNSUN strains.

1027 **(E)** Heatmap showing non-conversion rates of small non-coding RNA positions methylated in
1028 stoichiometry higher than 50%.

1029 Data information: In (A, B, C, D, E), n = 3 independent biological replicates.
1030

1031 **Figure 3. NSUN-4 is a dual tRNA/rRNA methyltransferase in *C. elegans*.**

1032 **(A)** RNA bisulfite sequencing map for mitochondrial tRNA Met-CAU in wild type (top) and
1033 noNSUN (bottom) strains. Each row represents one sequence read and each column one
1034 cytosine.

1035 **(B)** Percent identity matrix of human NSUN proteins according to the Clustal Omega multiple
1036 alignment tool.

1037 **(C, D)** Targeted bisulfite-sequencing heat map showing non-conversion rates of cytosines in
1038 mitochondrial tRNA Met-CAU (C) and mitochondrial 18S rRNA (D). Each row represents one
1039 genetic strain analysed and each column represents one cytosine.

1040 **(E)** Treefam phylogenetic tree based on sequence conservation of NSUN3 proteins in different
1041 model organisms. Bootstrap values are indicated on branches.

1042 Data information: In (A), a representative map of the replicates is shown, n = 3 independent
1043 biological replicates. In (C, D), the average of two experiments is plotted, n = 2 independent
1044 biological replicates, 10 clones sequenced per strain, per replicate. Similar effects were
1045 observed in all replicates analysed.
1046

1047 **Figure 4. Loss of $m^5C$ leads to a temperature-sensitive reproductive phenotype.**

1048 **(A)** Body length of individual *nsun* mutants throughout development (n = 44,7,7,7,8,8) in ~4
1049 hour windows. L1-L4 refers to the larval stages, YA and Ad to young adult and adult,
1050 respectively.
1051 **(B)** Size of mutant *nsun* strains at young adult and egg-laying stages. Approximately 100
1052 synchronised young adults of each strain were measured. Images were processed using custom
1053 algorithms to recognize *C. elegans* and measure their cross-sectional area.
1054 **(C, D)** Viable progeny counts of wild-type and *nsun* mutant strains at 20°C (C) and of wild-
1055 type and noNSUN strains at 20°C and 25°C (D). Automatic counting was done using a Matlab
1056 script which processed plate images in real-time.
1057 Data information: In (A), error bars indicate the 95% confidence interval of the median. In (C),
1058 data are presented as mean ± SEM, One-way ANOVA. In (D), data are presented as mean ±
1059 SEM, unpaired two-tailed Student's t-test.
1060
1061 **Figure 5. Loss of $m^5C$ impacts translation efficiency of leucine and proline codons.**
1062 **(A)** Fraction of polysomal ribosomes quantified from polysome profiles in the wild type and
1063 noNSUN strains subject to a 4 h heat shock at 27°C. ns = non-significant.
1064 **(B)** Heatmap showing P-site codon occupancy according to the colour scale at 20°C and 27°C.
1065 Red and blue refer to enhanced and reduced codon occupancy, respectively, in the noNSUN
1066 strain relative to wild type. Leucine and proline codons are marked in red.
1067 **(C)** Ribosome-protected fragment (RPF) counts in each sample plotted along *ife-1* and *pat-10*
1068 CDS. Vertical grey lines indicate UUG codons.
1069 **(D)** Translation efficiency of UUG-enriched, leucine-enriched, proline-enriched and random
1070 genes in each sample. A gene was considered enriched in a certain codon when the proportion
1071 of this codon in the gene was at least 3-fold higher than the proportion of the same codon across
1072 the transcriptome.
1073 Data information: In (A, B, C, D, E), n = 3 biological replicates. In (A), data are presented as
1074 mean ± SEM, unpaired two-tailed Student's t-test. In (D), boxplots show the median (central
1075 band) and IQR (boxes) ± 1.5 x IQR (whiskers), Welch's t-test, p-value < 0.05.
1076
1077
1078 **EXPANDED VIEW FIGURE LEGENDS**
1079
1080 **Figure EV1 | Related to Figure 2. Enzymatic specificity of NSUN proteins in *C. elegans*.**
1081 **(A, B, C)** Determination of enzymatic specificity of 26S rRNA C2381 (A), 26S rRNA C2982

1082 (B) and tRNA Leu-CAA C34 and C48 (C) methylation by targeted bisulfite-sequencing. Each
1083 column represents one cytosine in the sequence of interest; each line represents one clone
1084 sequenced. Enzymatic specificity of C2381 and C2982 in *C. elegans* has been independently
1085 demonstrated in other publications (Schosserer *et al*, 2015; Heissenberger *et al*, 2020).
1086
1087 **Figure EV2 | Related to Figure 2. Predicted secondary structures of $m^5C$-methylated**
1088 **ncRNAs.** Red dot indicates the methylated position. Structures predicted by the Predict a
1089 Secondary Structure Web Server (David Mathews Lab, University of Rochester) as the lowest
1090 free energy structures generated using default data.
1091
1092 **Figure EV3 | Related to Figure 5. Differentially transcribed and translated genes upon**
1093 **loss of $m^5C$ at different temperatures. (A, B)** Heatmaps and gene ontology enrichment
1094 (biological process) analysis for the comparison between wild type and noNSUN samples.
1095 Panel (A) shows RNA-seq (scaled normalised expression) and panel (B) shows Ribo-seq
1096 (scaled normalised RPFs). Sets of significant non-redundant GO terms are clustered according
1097 to semantic similarity; size indicates the frequency of the GO term in the underlying database
1098 WT = wild type; n = 3 biological replicates.
1099
1100 **Figure EV4 | Related to Figure 5. Codon occupancy analyses.**
1101 **(A)** Fold change of P-site codon occupancy in noNSUN over wild type samples at 20°C and
1102 27°C. p-values for the fold change occupancy of each codon are indicated in a heatmap below
1103 the graph, where asterisks indicate statistical significance. n = 3 biological replicates.
1104 **(B)** Representative examples of UUG codon occupancy in different affected genes. Ribosome-
1105 protected fragment counts (RPF) plotted along the gene's CDS. Vertical grey lines indicate
1106 UUG codons. n = 3 biological replicates.
1107 Data information: In (A), $p < 0.05$, t-test.
1108
1109 **Figure EV5 | Related to Figure 5. Translation efficiency of leucine and proline-enriched**
1110 **transcripts.** Translation efficiency of genes with increasing enrichment for leucine (top) or
1111 proline codons (bottom). Boxplots show the median (central band) and IQR (boxes) ± 1.5 x
1112 IQR (whiskers). n = 3 biological replicates.

# FIGURE 1

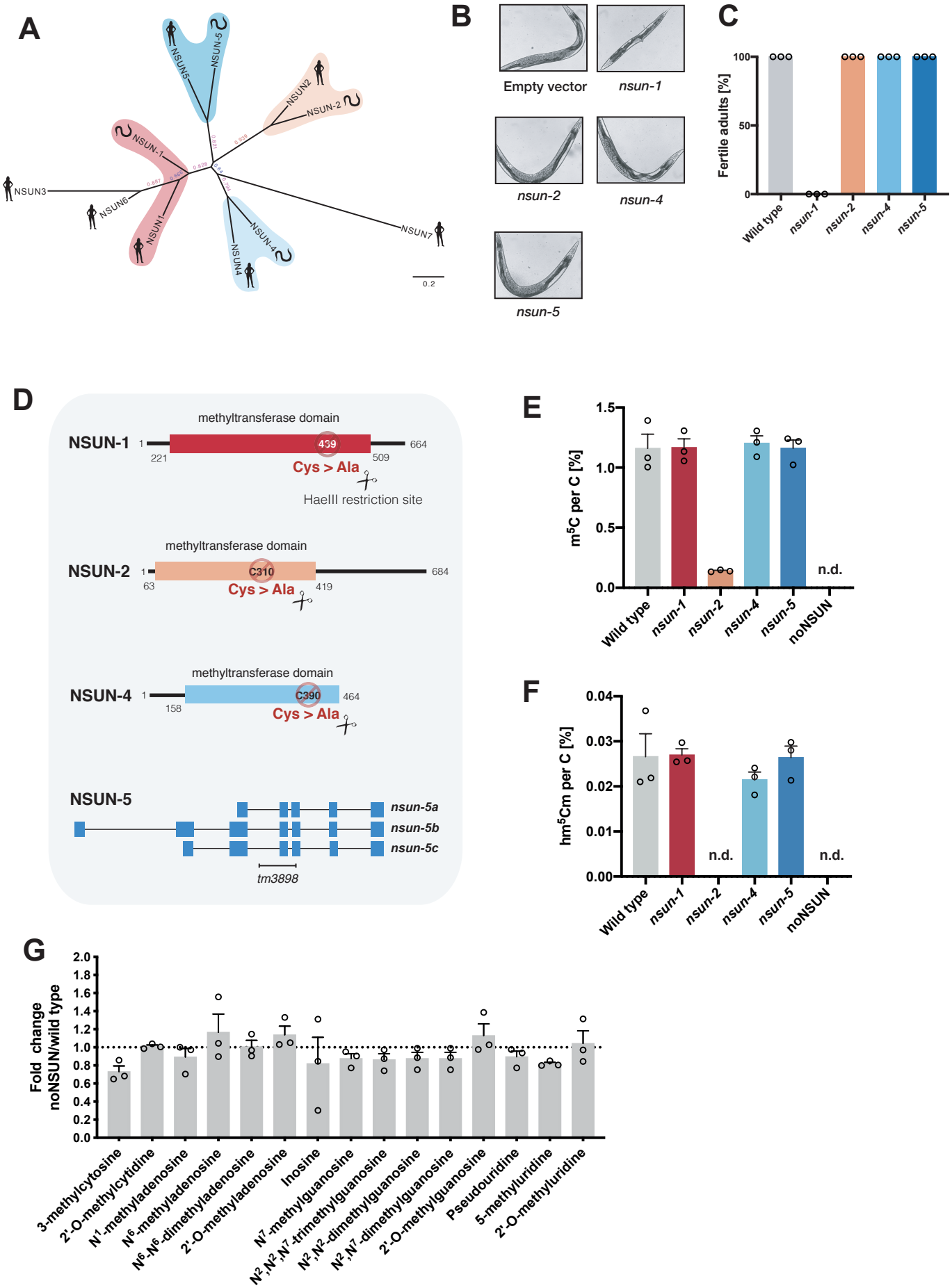
A
NSUN5
NSUN-5
NSUN2
NSUN-2
NSUN-1
NSUN3
NSUN6
NSUN1
NSUN4
NSUN-4
NSUN7
0.2
B
Empty vector
nsun-1
nsun-2
nsun-4
nsun-5
C
Fertile adults [%]
100
50
0
Wild type
nsun-1
nsun-2
nsun-4
nsun-5
D
methyltransferase domain
NSUN-1
1
221
439
509
664
Cys > Ala
HaeIII restriction site
methyltransferase domain
NSUN-2
1
63
C310
419
684
Cys > Ala
methyltransferase domain
NSUN-4
1
158
C390
464
Cys > Ala
NSUN-5
nsun-5a
nsun-5b
nsun-5c
tm3898
E
m5C per C [%]
1.5
1.0
0.5
0.0
n.d.
Wild type
nsun-1
nsun-2
nsun-4
nsun-5
noNSUN
F
hm5Cm per C [%]
0.04
0.03
0.02
0.01
0.00
n.d.
n.d.
Wild type
nsun-1
nsun-2
nsun-4
nsun-5
noNSUN
G
Fold change noNSUN/wild type
2.0
1.8
1.6
1.4
1.2
1.0
0.8
0.6
0.4
0.2
0.0
3-methylcytosine
2'-O-methylcytidine
N1-methyladenosine
N6-methyladenosine
N6-N6-dimethyladenosine
2'-O-methyladenosine
Inosine
N7-methylguanosine
N2,N2,N7-trimethylguanosine
N2,N2-dimethylguanosine
N2,N7-dimethylguanosine
2'-O-methylguanosine
Pseudouridine
5-methyluridine
2'-O-methyluridine

# FIGURE 2

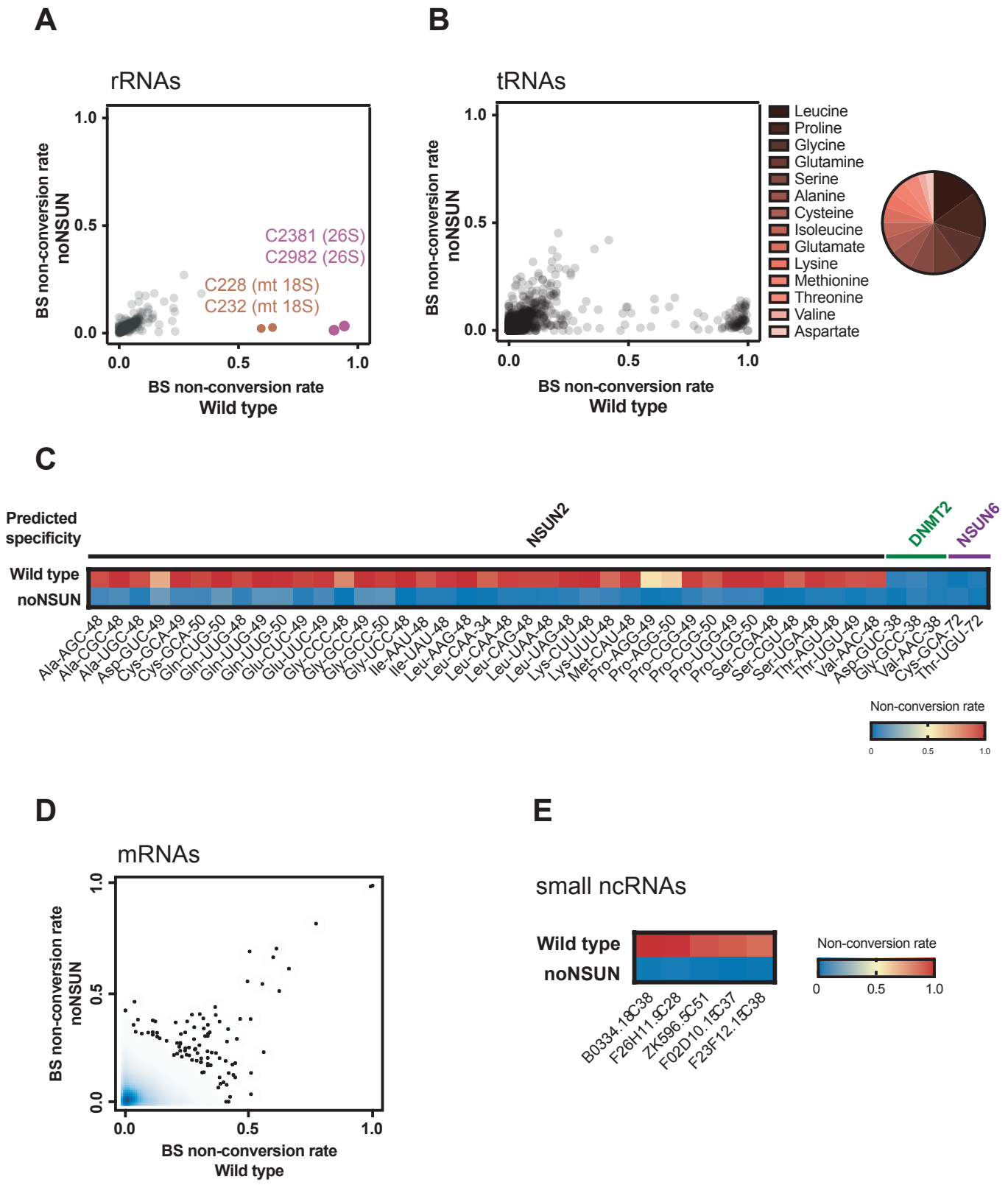
A
rRNAs
BS non-conversion rate noNSUN
BS non-conversion rate Wild type
C2381 (26S)
C2982 (26S)
C228 (mt 18S)
C232 (mt 18S)
B
tRNAs
Leucine
Proline
Glycine
Glutamine
Serine
Alanine
Cysteine
Isoleucine
Glutamate
Lysine
Methionine
Threonine
Valine
Aspartate
C
Predicted specificity
NSUN2
DNMT2
NSUN6
Wild type
noNSUN
Ala-AGC-48
Ala-CGC-48
Ala-UGC-48
Asp-GUC-49
Cys-GCA-49
Cys-GCA-50
Gln-CUG-50
Gln-UUG-48
Gln-UUG-49
Gln-UUG-50
Glu-CUC-49
Glu-UUC-49
Gly-CCC-48
Gly-GCC-48
Gly-GCC-49
Gly-GCC-50
Gly-UCC-48
Ile-AAU-48
Ile-UAU-48
Leu-AAG-48
Leu-CAA-34
Leu-CAA-48
Leu-CAG-48
Leu-UAA-48
Leu-UAG-48
Lys-CUU-48
Lys-UUU-48
Met-CAU-48
Pro-AGG-49
Pro-AGG-50
Pro-CGG-49
Pro-CGG-50
Pro-UGG-49
Pro-UGG-50
Ser-CGA-48
Ser-CGU-48
Ser-UGA-48
Thr-AGU-48
Thr-UGU-49
Val-AAC-48
Asp-GUC-38
Gly-GCC-38
Val-AAC-38
Cys-GCA-72
Thr-UGU-72
Non-conversion rate
D
mRNAs
BS non-conversion rate noNSUN
BS non-conversion rate Wild type
E
small ncRNAs
Wild type
noNSUN
B0334.18C38
F26H11.9C28
ZK596.5C51
F02D10.15C37
F23F12.15C38
Non-conversion rate

# FIGURE 3

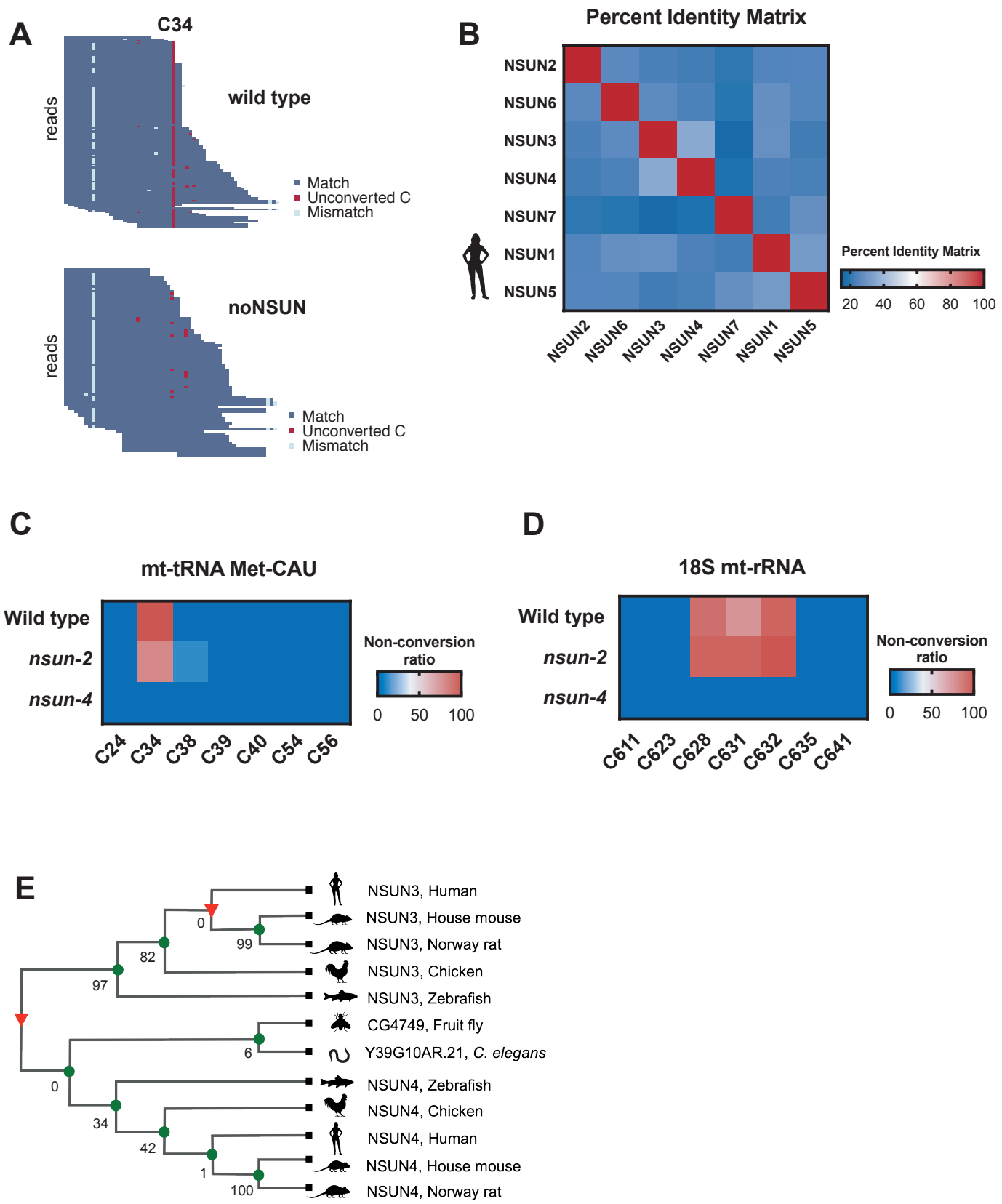
A
C34
reads
wild type
Match
Unconverted C
Mismatch
reads
noNSUN
Match
Unconverted C
Mismatch
B
Percent Identity Matrix
NSUN2
NSUN6
NSUN3
NSUN4
NSUN7
NSUN1
NSUN5
Percent Identity Matrix
20 40 60 80 100
C
mt-tRNA Met-CAU
Wild type
nsun-2
nsun-4
C24 C34 C38 C39 C40 C54 C56
Non-conversion ratio
0 50 100
D
18S mt-rRNA
Wild type
nsun-2
nsun-4
C611 C623 C628 C631 C632 C635 C641
Non-conversion ratio
0 50 100
E
NSUN3, Human
NSUN3, House mouse
NSUN3, Norway rat
NSUN3, Chicken
NSUN3, Zebrafish
CG4749, Fruit fly
Y39G10AR.21, C. elegans
NSUN4, Zebrafish
NSUN4, Chicken
NSUN4, Human
NSUN4, House mouse
NSUN4, Norway rat
0
99
82
97
6
0
34
42
1
100

# FIGURE 4

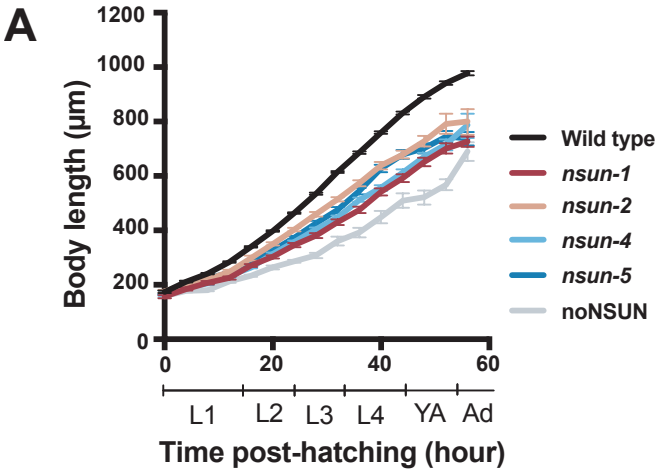
A
Body length (µm)
1200
1000
800
600
400
200
0
0
20
40
60
L1
L2
L3
L4
YA
Ad
Time post-hatching (hour)
Wild type
nsun-1
nsun-2
nsun-4
nsun-5
noNSUN

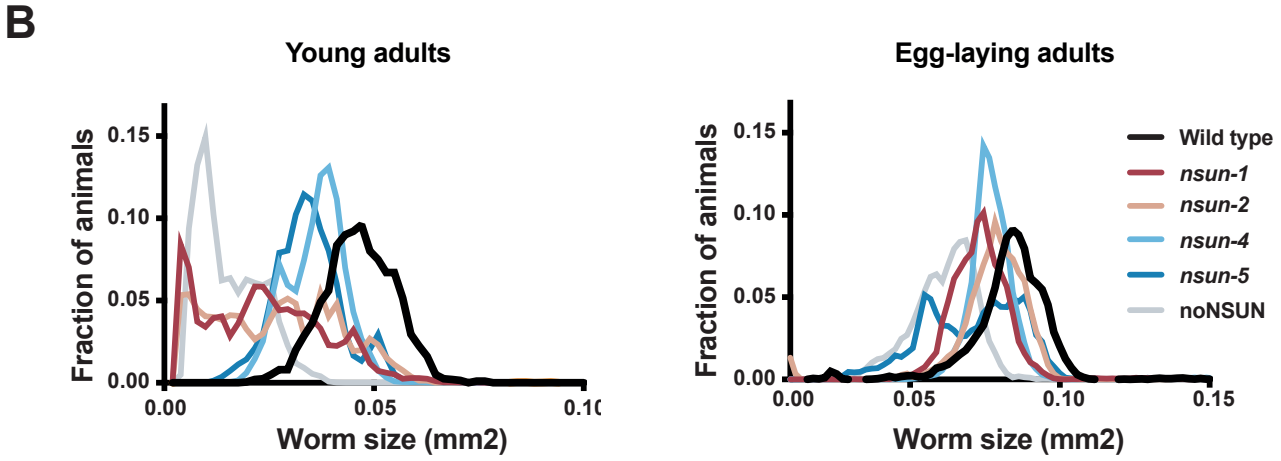
B
Young adults
Fraction of animals
0.15
0.10
0.05
0.00
0.00
0.05
Worm size (mm2)
Egg-laying adults
Fraction of animals
0.15
0.10
0.05
0.00
0.00
0.05
0.10
0.15
Worm size (mm2)
Wild type
nsun-1
nsun-2
nsun-4
nsun-5
noNSUN

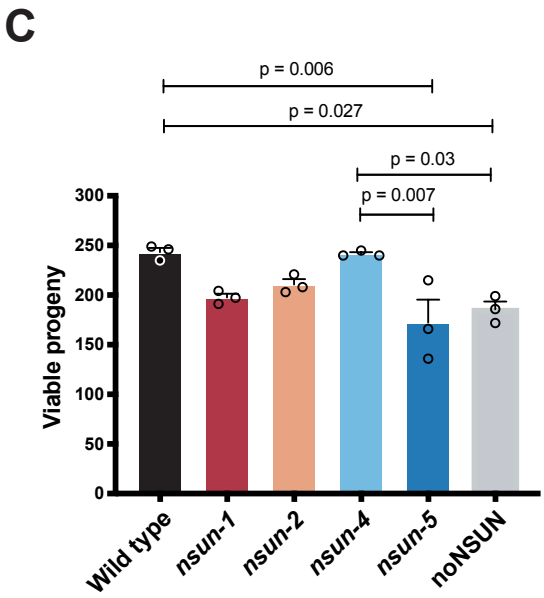
C
p = 0.006
p = 0.027
p = 0.03
p = 0.007
Viable progeny
300
250
200
150
100
50
0
Wild type
nsun-1
nsun-2
nsun-4
nsun-5
noNSUN

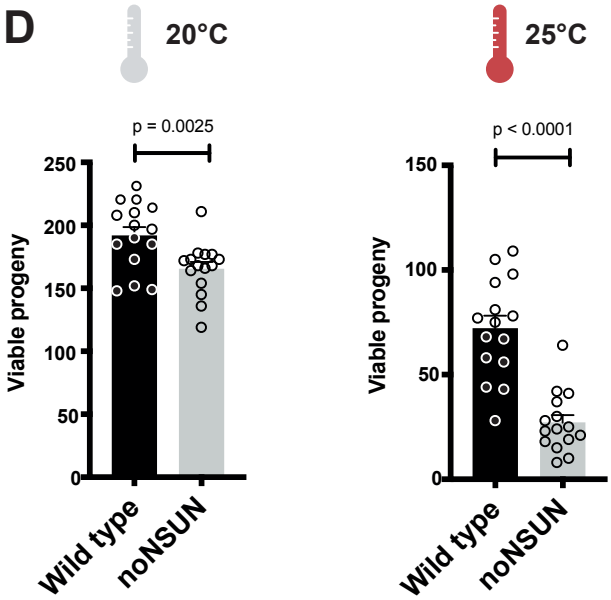
D
20°C
25°C
p = 0.0025
p < 0.0001
Viable progeny
250
200
150
100
50
0
Wild type
noNSUN
Viable progeny
150
100
50
0
Wild type
noNSUN

# FIGURE 5

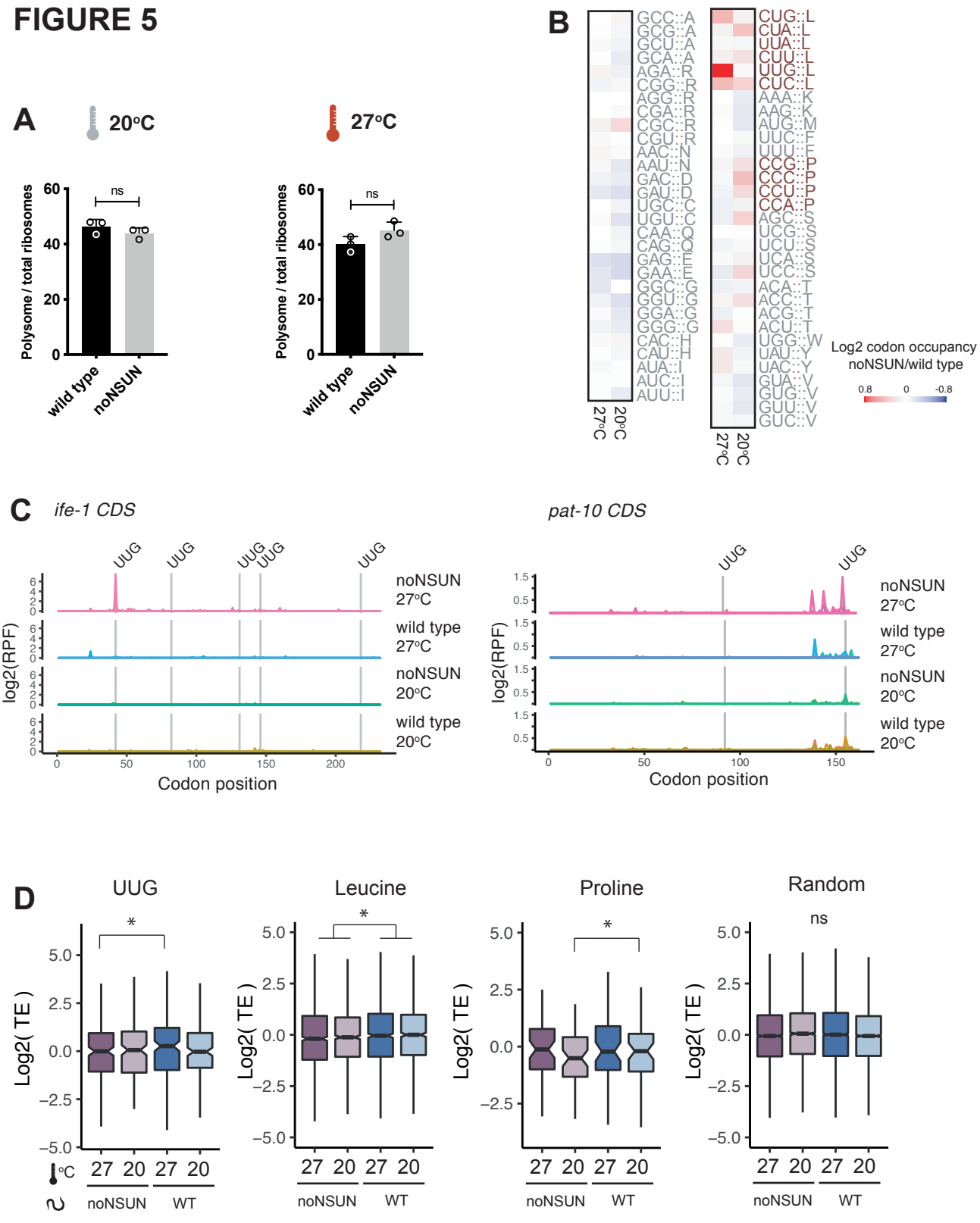
A
20°C
27°C
Polysome / total ribosomes
ns
wild type
noNSUN
B
GCC::A
GCG::A
GCU::A
GCA::A
AGA::R
CGG::R
AGG::R
CGA::R
CGC::R
CGU::R
AAC::N
AAU::N
GAC::D
GAU::D
UGC::C
UGU::C
CAA::Q
CAG::Q
GAG::E
GAA::E
GGC::G
GGU::G
GGA::G
GGG::G
CAC::H
CAU::H
AUA::I
AUC::I
AUU::I
CUG::L
CUA::L
UUA::L
CUU::L
UUG::L
CUC::L
AAA::K
AAG::K
AUG::M
UUC::F
UUU::F
CCG::P
CCC::P
CCU::P
CCA::P
AGC::S
UCG::S
UCU::S
UCA::S
UCC::S
ACA::T
ACC::T
ACG::T
ACU::T
UGG::W
UAU::Y
UAC::Y
GUA::V
GUG::V
GUU::V
GUC::V
27°C
20°C
Log2 codon occupancy
noNSUN/wild type
0.8
0
-0.8
C
ife-1 CDS
pat-10 CDS
UUG
log2(RPF)
noNSUN 27°C
wild type 27°C
noNSUN 20°C
wild type 20°C
Codon position
D
UUG
Leucine
Proline
Random
Log2( TE )
ns
°C
27 20 27 20
noNSUN
WT

# Figure EV1

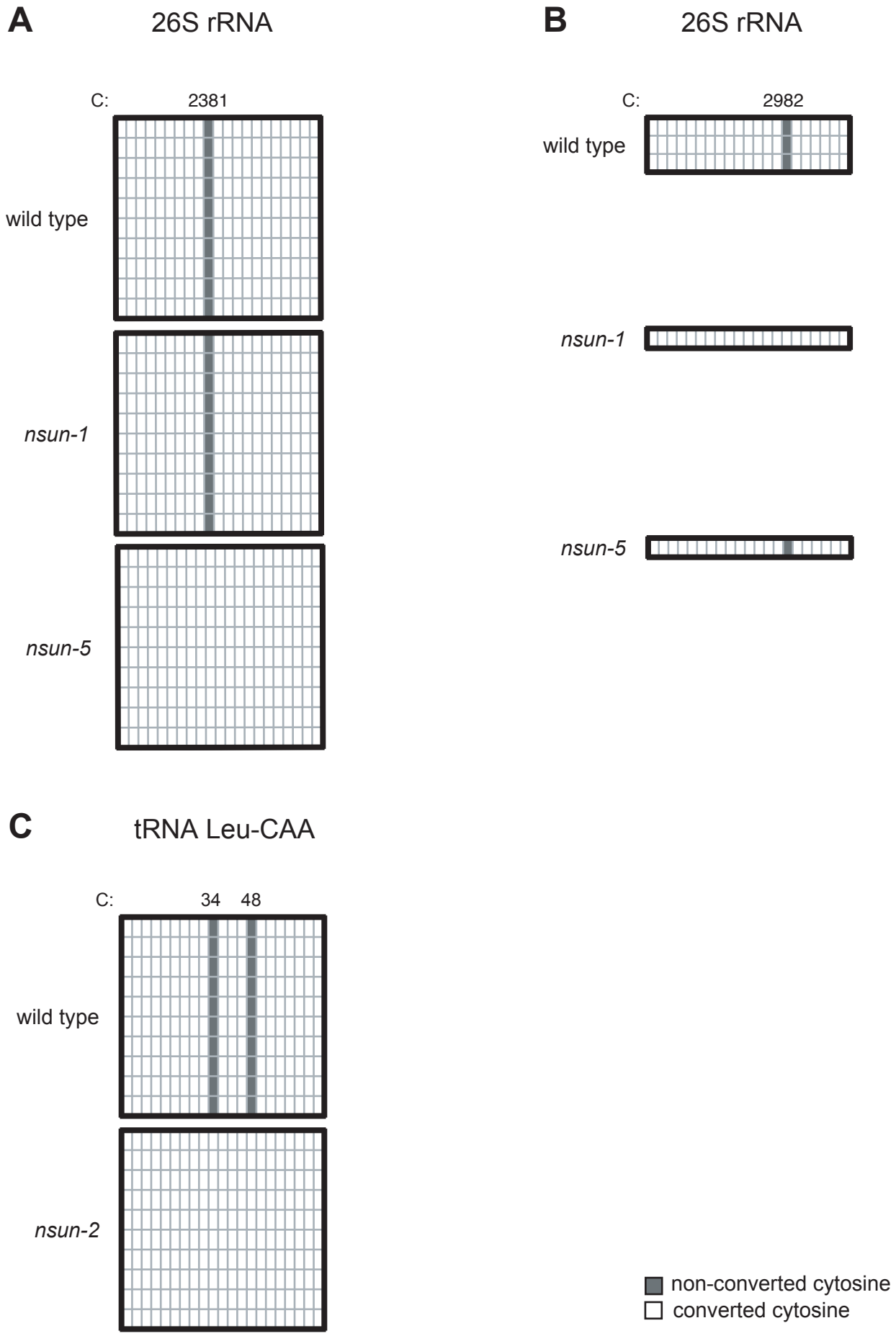
A
26S rRNA
C:
2381
wild type
nsun-1
nsun-5
B
26S rRNA
C:
2982
wild type
nsun-1
nsun-5
C
tRNA Leu-CAA
C:
34
48
wild type
nsun-2
non-converted cytosine
converted cytosine

# FIGURE EV2

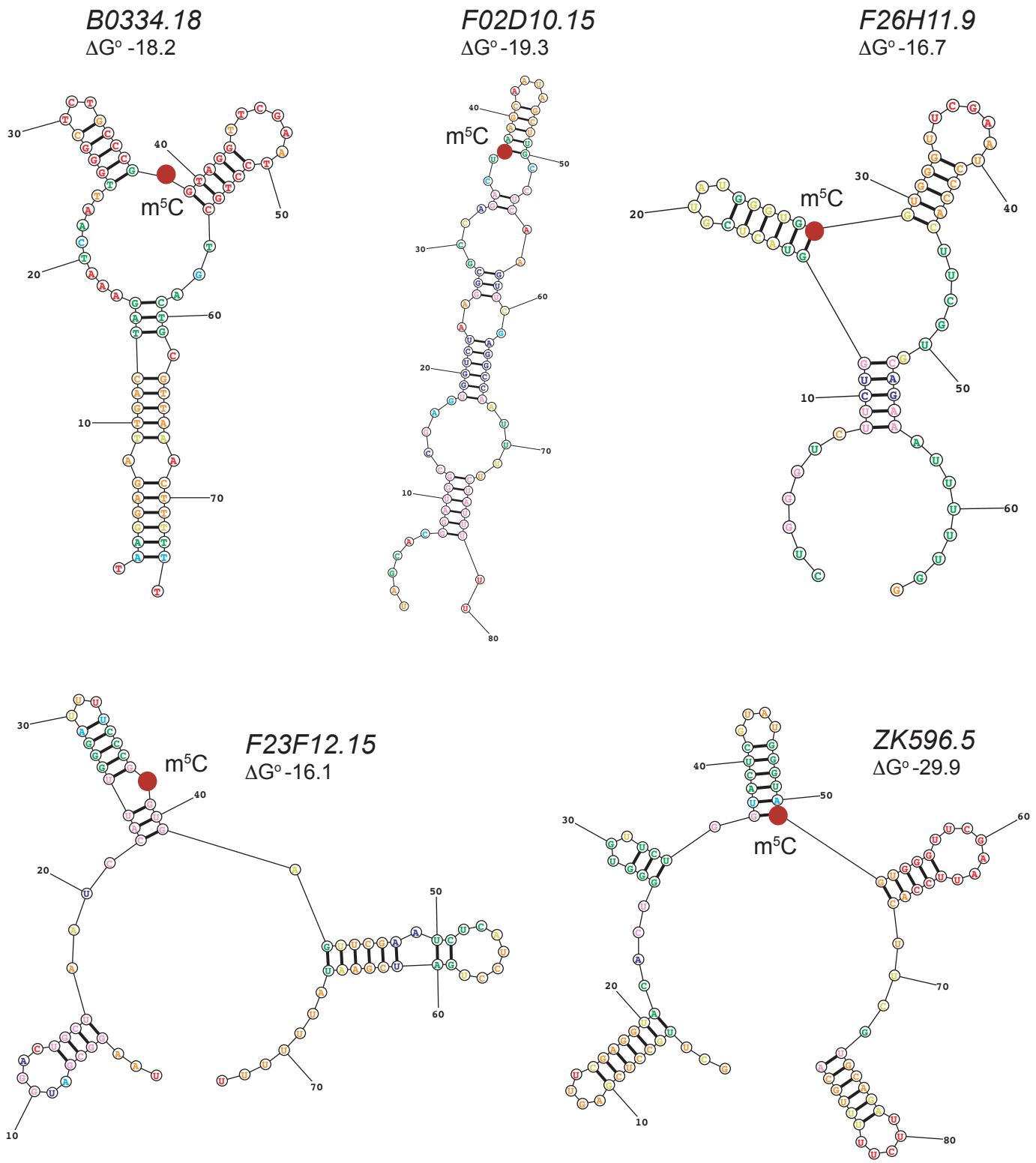


**Probability >= 99%**
**99% > Probability >= 95%**
**95% > Probability >= 90%**
**90% > Probability >= 80%**
**80% > Probability >= 70%**
**70% > Probability >= 60%**
**60% > Probability >= 50%**
**50% > Probability**

# FIGURE EV3

## A

### RNA-Seq

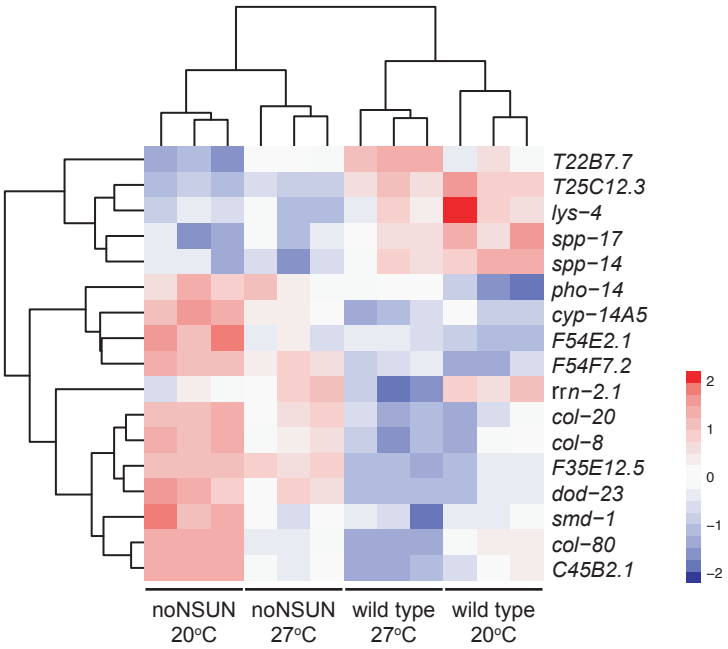


### GO Term: Molecular Functions

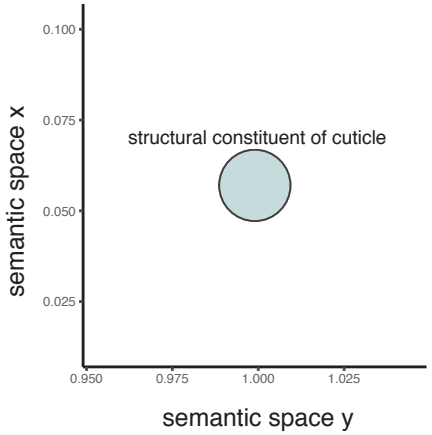


## B

### Ribo-Seq

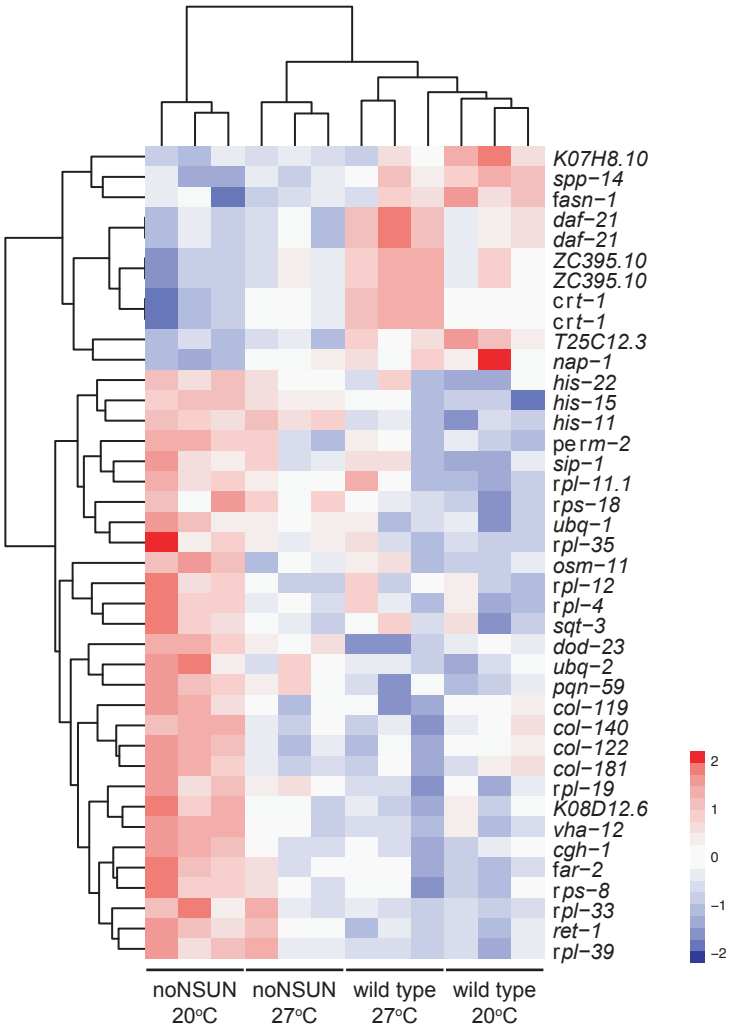


### GO Term: Molecular Functions

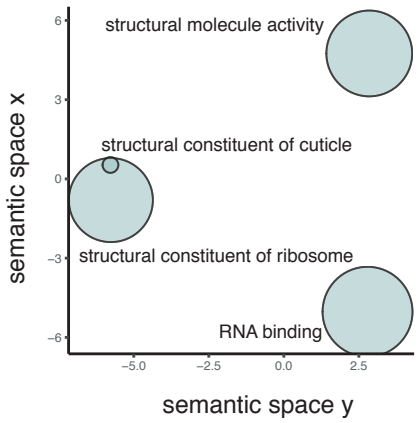

# FIGURE EV4

## A

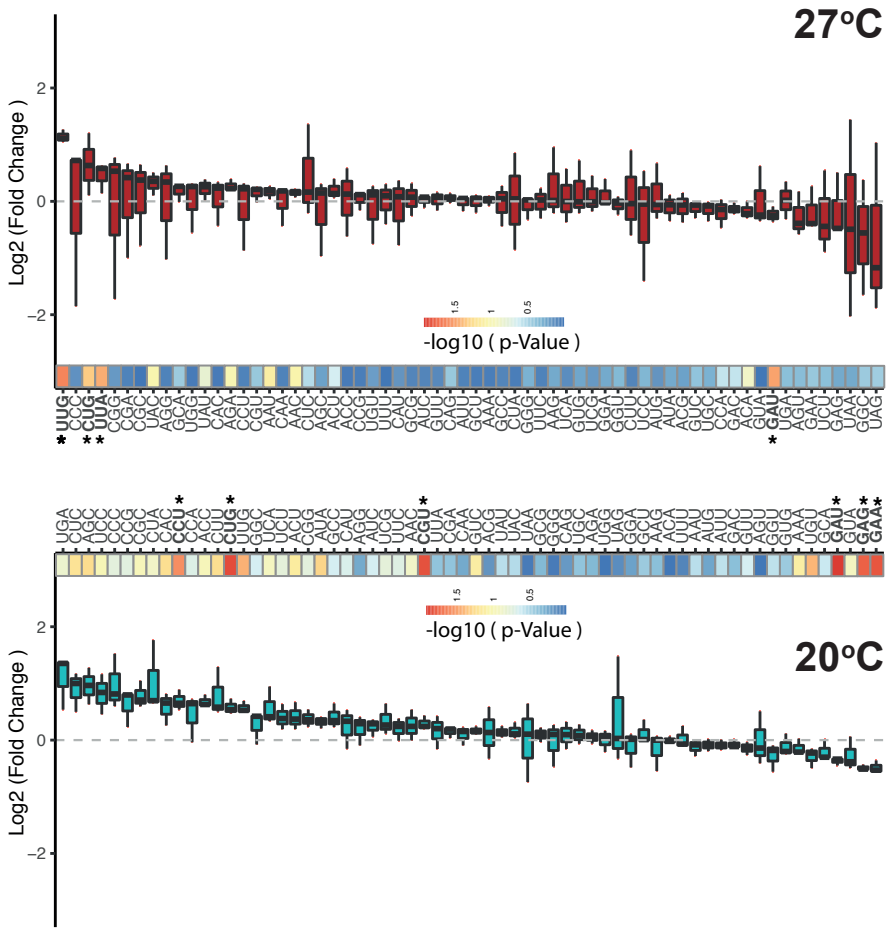


## B

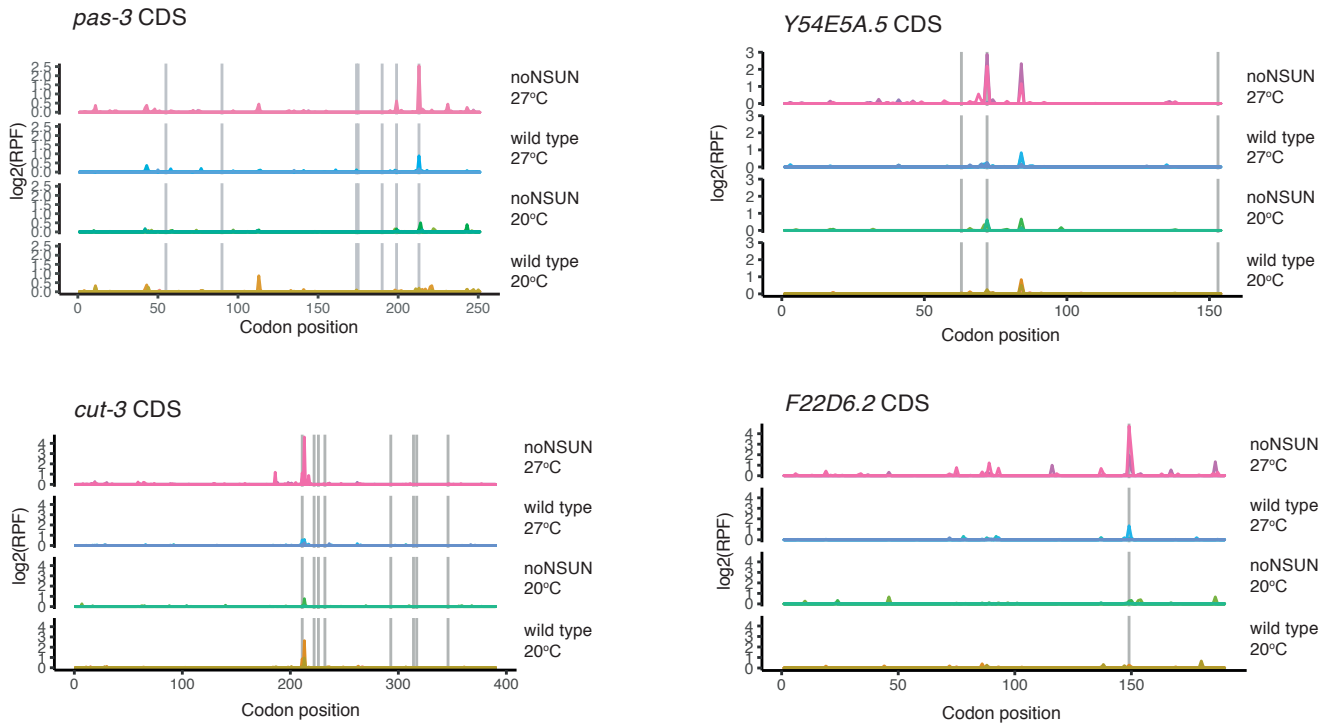

# FIGURE EV5

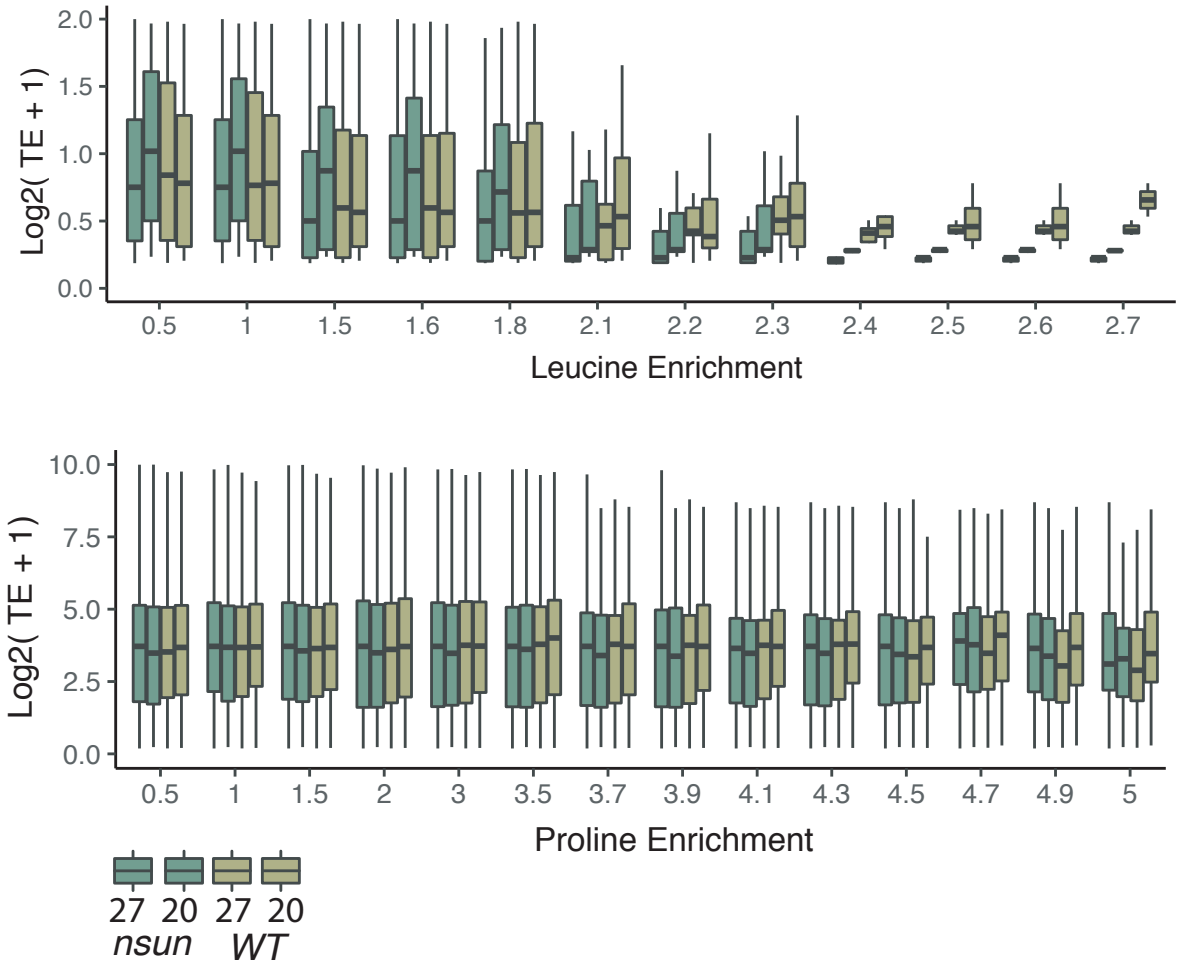
Log2( TE + 1)
2.0
1.5
1.0
0.5
0.0
0.5
1
1.5
1.6
1.8
2.1
2.2
2.3
2.4
2.5
2.6
2.7
Leucine Enrichment
Log2( TE + 1)
10.0
7.5
5.0
2.5
0.0
0.5
1
1.5
2
3
3.5
3.7
3.9
4.1
4.3
4.5
4.7
4.9
5
Proline Enrichment
27 20 27 20
nsun WT

***Appendix***

Navarro et al., Translational adaption to heat stress is mediated by RNA 5-methylcytosine in *Caenorhabditis elegans*

Contents:

# FIGURE S1

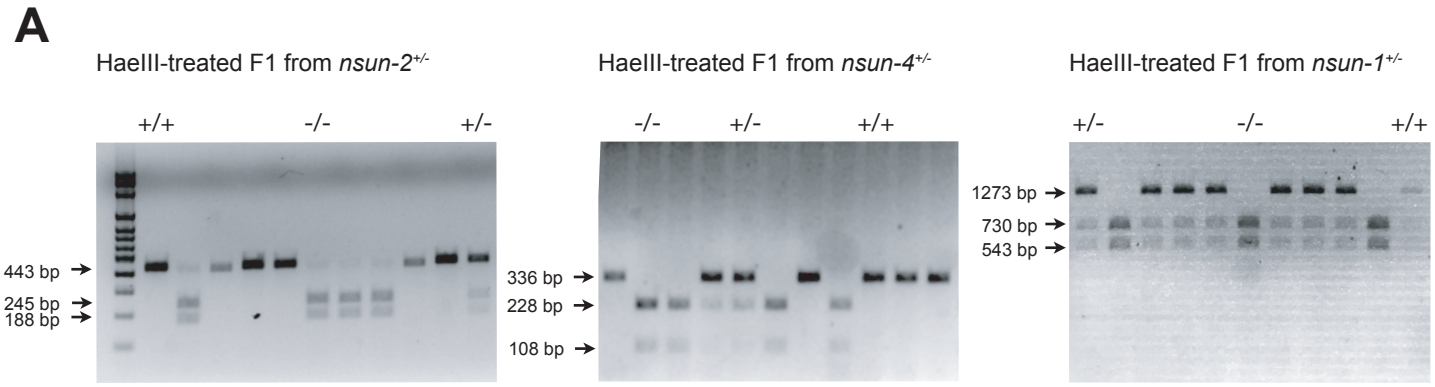


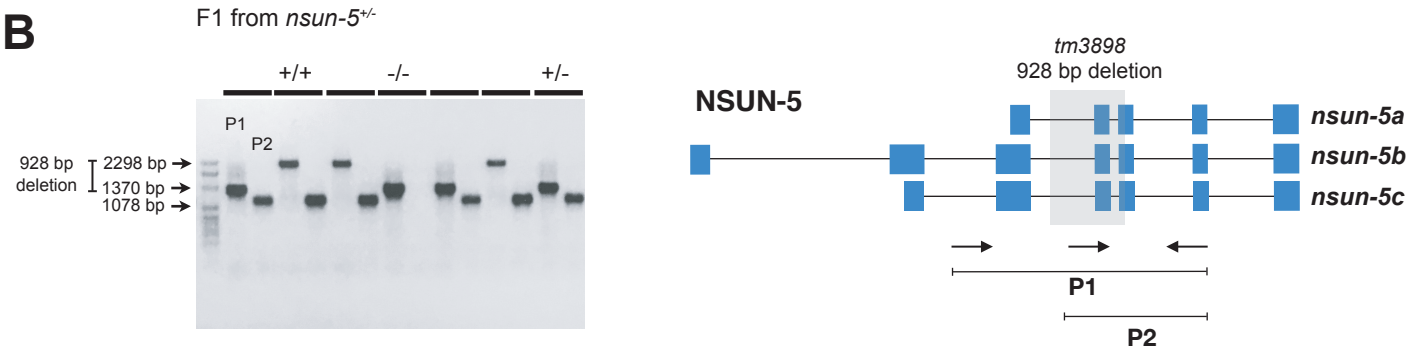


**Figure S1 | Related to Figure 1. Genotyping of *nsun* mutants.**
**(A)** HaeIII-treated DNA agarose gel showing genotypes of F1 individuals from heterozygous *nsun-1, nsun-2* and *nsun-4* mutants.
**(B)** DNA agarose gel showing genotypes of F1 individuals from a heterozygous *nsun-5* mutant; diagram showing primers used for genotyping of *nsun-5* mutation.

# FIGURE S2

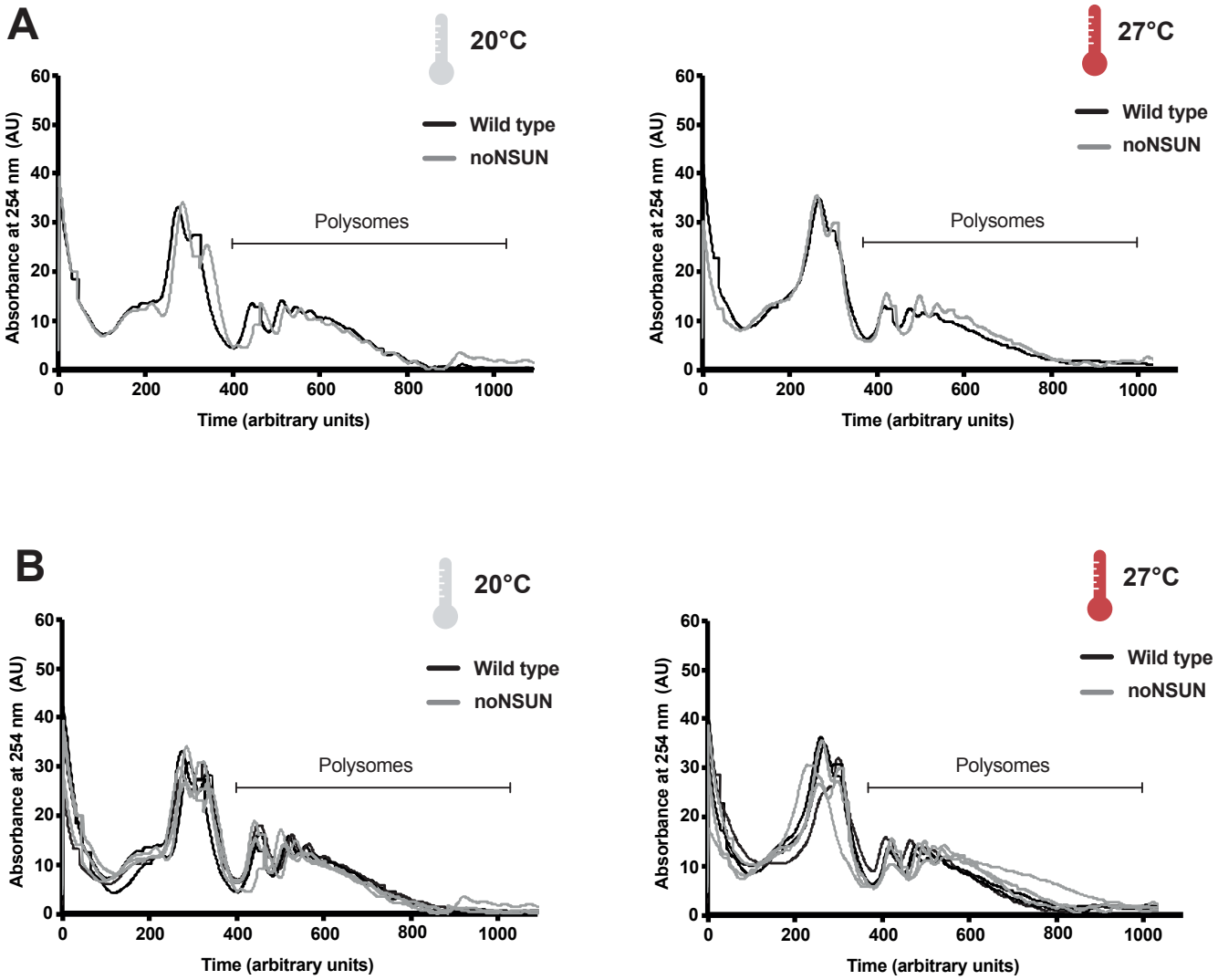


**Figure S2 | Related to Figure 5A. Polysome profiles of wild type and noNSUN animals subjected or not to a heat shock at 27°C**

**(A)** Representative polysome profiles of wild type and noNSUN strains at 20°C (left) and 27°C (right). Graphs normalised by the total area under the curve.

**(B)** Polysome profiles of wild type and noNSUN strains at 20°C (left) and 27°C (right) in triplicates. Graphs normalised by the total area under the curve.

Data information: n = 3 biological replicates.

# FIGURE S3

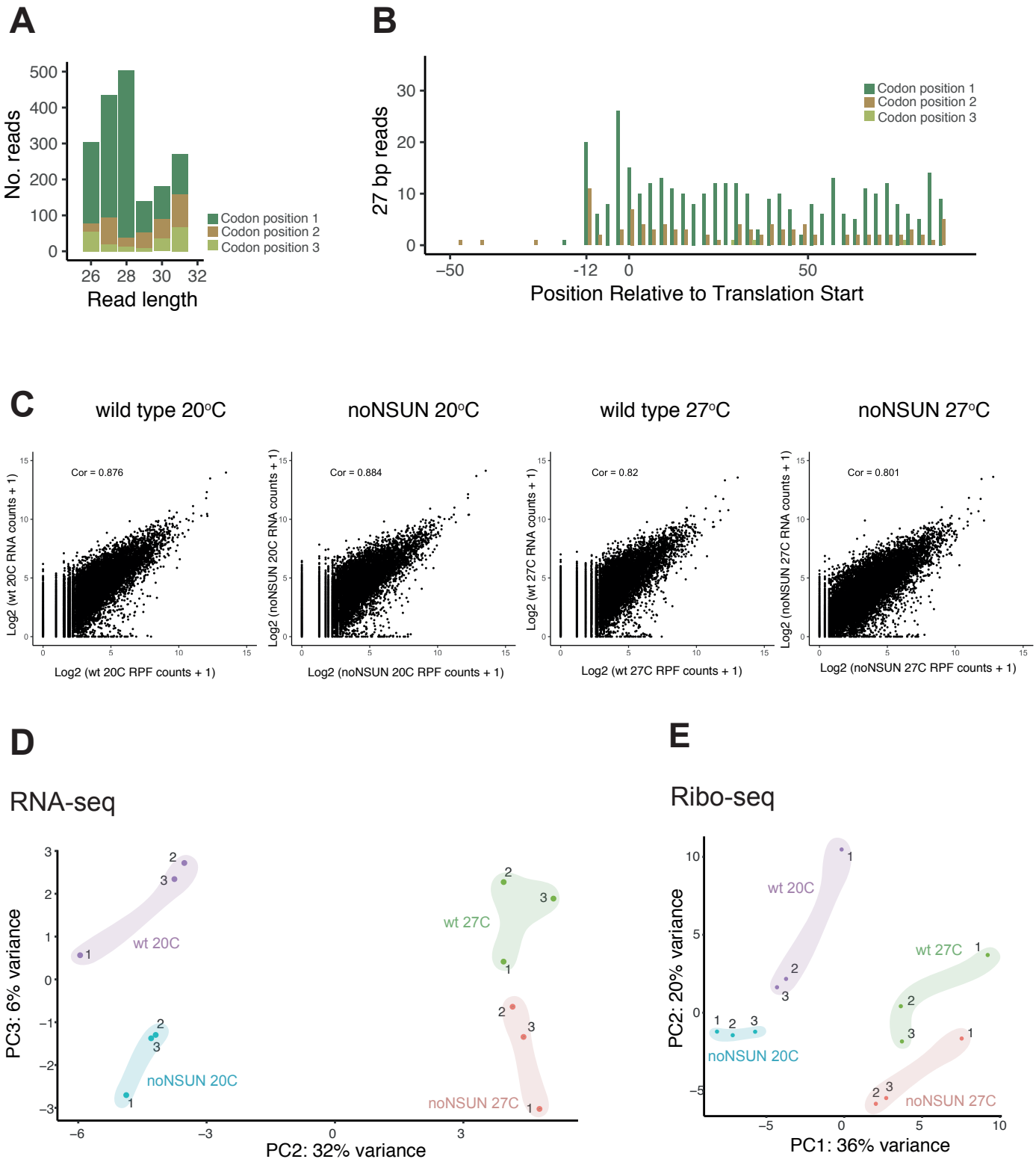


**Figure S3 | Related to Figure 5. Quality assessment of ribosome profiling data.**
**(A)** Number of reads aligning the to the CDS in each frame after length stratification. The frame of the 5′ nucleotide is shown.
**(B)** Representative meta-gene plot for 27 bp reads showing 3-nt periodicity. Number of reads for each codon position coloured according to the frame of their 5′ base relative to the CDS.
**(C)** Scatter plots showing the correlation between transcripts and footprints abundance for each gene at the indicated samples. Pearson correlation coefficient (r) is shown.
**(D)** PCA plot of RNA-seq counts for the 2000 genes with the highest variance.
**(E)** PCA plot of Ribo-seq counts for the 2000 genes with the highest variance.
Data information: n = 3 biological replicates.

# FIGURE S4

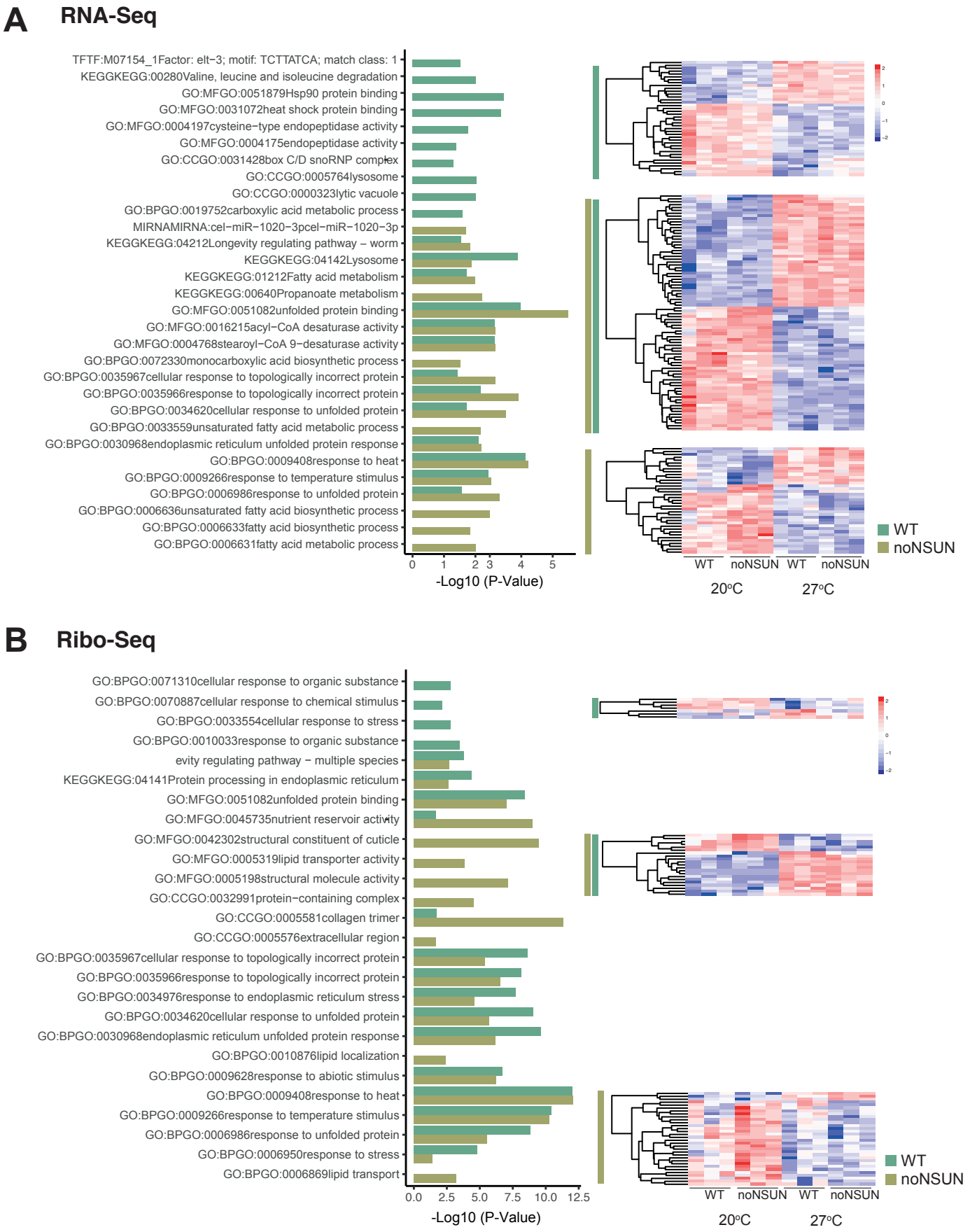


**Figure S4 | Related to Figure 5. Differentially transcribed and translated genes in wild type and noNSUN strains upon heat shock. (A, B)** Heatmaps and gene ontology enrichment (biological process) analysis for the comparison between 20°C and 27°C in the wild type and noNSUN samples. (A) shows RNA- seq (scaled normalised expression) and (B) shows Ribo-seq (scaled normalised RPFs). Data information: n = 3 biological replicates. WT = wild type.